Structure Determination of Polymer Nanocomposites by Small Angle Scattering

Julian Oberdisse, Wim Pyckhout-Hintzen, Ekkehard Straube

Structure Determination of Polymer Nanocomposites by Small Angle Scattering

Julian Oberdisse[1], Wim Pyckhout-Hintzen[2], Eckehard Straube[3]

[1] Laboratoires de Colloïdes, Verres et Nanomatériaux, CNRS/ Université Montpellier II, France
[2] Institut für Festkörperforschung, Forschungszentrum Jülich, Germany
[3] Martin-Luther Univ. Halle, FB Physik, D-06099 Halle-Saale, Germany

16/05/2007

Abstract

The characterization of the structure of polymer nanocomposites by the techniques of small-angle scattering of neutrons and X-rays is reviewed. Within a concise introduction to elastic small-angle scattering, the basics of shape, structure, and interactions of particles are presented, as well as the scattering from polymer chains.

The scattering properties of polymer chains can be described within models that can also account for stress-strain properties. In neutron scattering, stretched polymer chains and their fluctuation width can be directly accessed by taking advantage of the difference in the scattering length between H and D atoms. Further, SANS can equally cope with the mounting interest in the characterization of polymers in nowadays popular multiphase materials. Using contrast matching or a combination of two probes, i.e. neutrons and x-rays, the solid phase can be made invisible or visible. This allows to extract new structural information about the rubbery matrix that could not be obtained separately by other methods.

Current literature on filler scattering in polymer nanocomposites will be reviewed. The most common fillers where scattering has been shown to be decisive are carbon black, silica, polymeric fillers, and, to a lesser extent, clay. Scattering is a powerful tool to analyse the filler structure in a non destructive way, in the dry (pure filler) state, in solution, or inside macroscopically thick nanocomposite samples. The scattered intensity is obtained as an average over the complete sample, thereby decreasing the impact of possible artefacts as it might be the case in direct-space imaging. In this review part, it is attempted to give an overview of the morphology of the hard component typically encountered in filled polymer systems, its modes of deformation as the sample is deformed, as well as a summary of possible routes of data interpretation and modelling.

Table of Contents

I. Introduction

The great practical importance of polymer composites materials is due the modification, and usually improvement, of the properties of the pure polymer. The improvement of mechanical properties, although very different in nature according to the application of interest and the polymer used, is generally termed the reinforcement effect [1, 2]. This effect includes phenomena as various as the increase of tensile strength and maximum elongation of elastomers, the reduction of brittleness and improvement of fracture toughness, or better abrasion resistance for car tires [3, 4]. In general, mechanical reinforcement has been defined as all mechanisms that introduce energy dissipation or storage [5]. Other goals are specific barrier or optical properties, or simply lower production costs, which is a non negligible factor given the industrial tonnage of composites.

This review focuses on structure determination in polymer nanocomposites by scattering methods, namely Small Angle Neutron Scattering and Small Angle X-ray scattering. We concentrate on the case of soft and continuous polymer matrices with inclusions of hard, nanometric filler particles, among which carbon black, silica and silicates are the most common ones [6, 7]. In all of the applications cited above, the structure of these inclusions is essential. Optical properties of composites, like light transmittance, can be optimised only for well-dispersed submicron particles, which is of increasing importance in a world dominated by appearance and design. More seriously, barrier properties, e.g., can be improved with a specific spatial distribution of platelet-like particles (clays), because this increases the tortuosity of the diffusive paths that molecules need to follow across the material. Another example is fracture toughness, which is usually increased by the introduction of heterogeneities in the sample. Stress release is then obtained through the formation of many small cracks, which can not grow to a catastrophic size if they encounter tougher regions [4]. Hence the dispersion, or the structure, of hard regions in the nanocomposite is crucial, and a large part of this review will be dedicated to it. As additional examples, one may mention filler particles which can interact, e.g. aggregate, or form percolating hard networks at high filler volume fractions [8]. These structures can carry stress, or introduce dissipative mechanisms, like aggregate break-up and reorganization, which contribute to the reinforcement effect. In these cases, it is thus important to be able to characterize the filler structure, and follow its evolution under deformation.

Besides the filler structure, the configurations of the polymer chains inside a nanocomposite can also be investigated by scattering, and in particular neutron scattering [9, 10]. Statistical mechanical theories relate the configuration in space to the stress carried by polymer chains [11], and this may be used to connect structural observations on the nanoscale with mechanical properties. The characterization of chain configurations under deformation might then allow a molecular understanding of mechanical reinforcement, e.g. the increase in tensile strength of filled elastomers. This subject is still open, and we can outline at least two scenarios which have not been checked and understood in detail so far. First, at low filler volume fractions, the reinforcement is in general hydrodynamic [2, 12-14]. This should induce the deformation of the stress field in the polymer around the filler particles, which in turn should be seen in scattering. Second, at higher volume fractions, hard filler structures can built up and can in principle contain soft polymer regions, so called occluded rubber, and protect them from macroscopic strain [15, 16]. Occluded rubber is thought to contribute

inasmuch as it increases the effective filler volume fraction, and this population should be visible as undeformed rubber even in a deformed state. To our knowledge, occluded rubber has been often invoked but its existence remains to be proven.

A field which we deliberately exclude from this review are interactions at the filler–polymer interface. Upon mixing polymer with filler, and especially carbon black, and extraction of the polymer with a good solvent afterwards, it is usually found that some polymer, called bound polymer (or bound rubber), can not be recovered [15]. This illustrates that there may be strong interactions between the filler and the chains. For some aspects of reinforcement, the polymer at the interface with the filler can dominate the mechanical response of the nanocomposite. This may be due to changes in dynamical properties, like the increase of the glass transition temperature T_g of the matrix polymer close to a hard surface, which increases the effective filler volume fraction and may move the system closer to mechanical percolation [17, 18]. Such studies rely on completely different experimental approaches, and dynamical processes are outside the scope of this contribution. Other interfacial mechanisms include the linking by coupling agents of the filler particle to the network, or the improved compatibility of the filler with the polymer by grafting polymer chains on the filler surface. In all of theses cases, it is interesting to directly access the structure of this polymer layer at the interface, and we will see that this is in principle possible with small angle scattering [19-21].

It will be shown in this chapter that scattering methods can be used to characterize the structure of both the polymer chains and the filler, at rest and in the deformed state. Before going into detail, a word of caution about ‘structure’ may be appropriate. In the filler literature, structure is usually associated with a high specific surface, i.e. a small primary particle. A high-structure carbon black, for instance, has high oil-adsorption characteristics. Such carbon black usually consist of aggregates of small primary particles, but fusion processes may finally transform it into big particle with many pores or voids. In scattering from colloidal particles, structure concerns the interaction between primary particles (e.g. silica spheres), mathematically expressed through the pair correlation function, the Fourier transform of which is measured in a scattering experiment. Dilute dispersions of primary particles are usually non-interacting, in the sense that there is no positional correlation between them. In contrary, attractive interactions may lead to aggregation, and repulsive interactions to positional ordering of the particles. Throughout this contribution, unless

specified otherwise, the word ‘structure’ refers thus to the positional correlations between particles and, on a bigger scale, aggregates.

The outline of this chapter is the following. We start with a quick introduction to the analysis of small angle scattering data in section II. Individual filler particles, such as they are present in dilute solution or composites, can be characterized in a straightforward manner by scattering experiments. Typically, their average mass, shape, size, and amount of surface can be read off from the scattered intensity, which is given by the particle form factor. The average scattering from chains can be described along the same lines, yielding chain statistics, mass, and radius of gyration. At higher filler volume fractions, particles can interact, the signature of which is described by the interparticle structure factor. If particles aggregate, the resulting clusters can be characterized in terms of their size, density, and possibly fractal dimension.

In the third section the scattering from polymer chains in filled networks and melts is reviewed. The statistical properties of the chains may be altered due to the presence of the filler particles, and the chain form factor, at rest and under deformation, can be measured by highlighting some chains in a contrast variation scattering experiment. In the fourth section, the structural characterization by small angle scattering of the filler particles in different polymer-filler systems is reviewed. This includes studies of model systems, like dispersion and aggregation of spherical particles, as well as layered silicates and carbon blacks, at rest and under deformation.

II. A Quick Guide to Data Analysis of Small Angle Scattering

There are many excellent textbooks on small angle scattering (SAS) in the field of colloids and polymers, which are the two building blocks of polymer nanocomposites we are interested in [22-25]. Here we will only recall the basics necessary for the understanding of the literature in the field.

II.1. Basics of Elastic Small Angle Scattering

There are two main techniques operational in the 1 to 100 nanometer range, Small Angle Neutron Scattering (SANS) and Small Angle X-ray Scattering (SAXS). SAXS uses

wavelengths of about one Ångstroem, and SANS up to one or (rarely) two nm for cold neutrons. These radiations differ in penetration of matter and in their energy, which is of importance for dynamic studies, but outside the scope of this chapter. The elastic interaction of these radiations with matter, X-rays with electrons and neutrons with the nuclei, respectively, is characterized by the coherent scattering length of each atom b, which can be looked up from tables (for neutrons) or calculated in the case of x-rays. Depending on the approach, assemblies of atoms, like molecules or colloidal particles, are described by the coherent scattering lengths b of the particles or by the scattering length density ρ, i.e. the sum of all the b's divided by the considered reference volume (which may be a chemically homogeneous particle):

$$\rho = \frac{\sum b_i}{V} \tag{1}$$

The index 'i' runs over all different scattering entities inside V. A two-component structure reduces then using the incompressibility condition to an isolated object against an invisible and structureless background. Intelligent labelling in the case of a three-component mixture as will be necessary in the case of blends with nanocomposites, can be thought of to limit the number of parameters as well as to match out any contributions of the unwanted, most of the time also uninteresting or unknown component. Structural analysis of polymer nanocomposites by small angle scattering is based on the variation of the scattering length density ρ(r) across the sample. In the case of particles in solution, in a polymer network or melt, the variation of ρ is naturally given by $\Delta\rho = \rho_{particle} - \rho_{matrix}$, which is called the contrast between the matrix and the particle. If one is interested in the conformation of a chain surrounded by other chains, the contrast must be created artificially. With neutrons, this is straightforward (although quite expensive), as deuterated chains have a high contrast in a hydrogenated environment. Samples with scattering length density variations on nanometer scales will scatter radiation. Their scattering power, expressed through the differential scattering cross section per unit volume $d\Sigma/d\Omega$, is usually given in cm^{-1}, also called 'in absolute units'. Alternatively, the total scattering cross section $d\sigma/d\Omega$ may also be used. $d\Sigma/d\Omega$ is determined in an experiment by measuring a neutron or photon flux (or better, current, i.e. a number per unit time) $I_{exp}(q)$ on a given detector element, followed by background subtraction and normalization:

$$I_{exp}(q) = I_{in} A \varepsilon \, T \, \Delta\Omega \, (d \, d\Sigma/d\Omega(q) + B) \qquad (2a)$$

where I_{in} is the incoming flux (number per unit time and area), A the illuminated section of sample, ε the detector efficiency, T the transmission, $\Delta\Omega$ the solid angle of the detector element, d the sample thickness, and B the background due to the sample environment (empty cell). The latter should not be confused with the incoherent background, which is inherent to the sample and which we suppose is subtracted properly in what follows. The scope of the process of 'data reduction' (or primary data treatment) is to get rid of all contributions of the experimental set-up, like the geometry or the incoming flux, and identify what is due to the structure of the sample, i.e. its scattering power, expressed through the differential scattering cross section. Due to this experimental origin, we have adopted in the following the somewhat sloppy denomination 'scattered intensity', or I(q), meaning in reality $d\Sigma/d\Omega$. The scattered intensity I(q), depends on the scattering vector q, which is related to the scattering angle Θ and the wavelength λ by

$$q = 4\pi/\lambda \sin \Theta/2 \qquad (2b)$$

The scattered intensity gives thus access to the typical $\Delta\rho$ variations, e.g. particle shapes, polymer conformations, and interactions between them. For the dedicated reader it should be clear that the same approach is applicable using X-rays if the coherent scattering length densities are replaced by the electron density together with the Thompson factor. For the sake of clarity this review is written around the neutron as probe. The density variation with electrons is much less and therefore SAXS analyses are restrained more or less to the simplest two-component cases. Nevertheless, it will be shown that a hybrid analysis (using additional x-ray data) of more complex neutron data can assist to distinguish between deformation mechanisms in both phases of the composites as well as to limit the number of unknowns, especially if contrast condition were not met ideally.

II.2 Form factors of particles and chains

If one incorporates a given type of filler particles inside a polymer matrix, one usually wishes to have some quantitative description of the filler itself. If it is chemically homogeneous and

inside the size window accessible with SAS, then a dilute solution or composite (i.e. where typical interaction distances are smaller than the average distance between particles, in practice with colloids of volume fraction usually less than approximately 1%) will scatter according to the following law:

$$I(q) = \Phi \, \Delta\rho^2 \, V \, F^2(q) \tag{3}$$

Here I(q) denotes the scattered intensity in absolute units (= $d\Sigma/d\Omega$), Φ is the volume fraction of the filler, $\Delta\rho$ its contrast with respect to its environment (matrix, solvent…), V the average volume of one particle, and $F^2(q)$ is called the normalized particle form factor (sometimes written P(q)). It is normalized because its low-q limit is one. F^2 can be calculated by Fourier transforming the density functions of the desired particle shapes. For monodisperse spheres of radius R, e.g., we obtain:

$$F^2(q) = 9\frac{(\sin(qR) - qR\cos(qR))^2}{(qR)^6} \tag{4}$$

This function is shown in Figure 1, as a function of the product qR. Together with eq.(3), this Figure illustrates that several key features of spherical and more generally globular objects can be determined by such a measurement. The low-q limit, e.g., if the intensity has been collected in absolute units, gives directly the average volume of the particles, and thus the particle mass. At intermediate q-values, the representation in log-log units emphasizes the sudden decrease of F^2 around q = 1/R. The onset of this decrease is traditionally described by a Guinier law, which can be obtained via a small angle development of eq.(4):

$$I = I_o \exp(-q^2 Rg^2/3) \tag{5}$$

The Guinier law introduces the radius of gyration of particles, which is related in the case of spheres by $Rg^2/R^2 = 3/5$. Simple geometric relations exist for different particle shapes. The Guinier law is therefore independent of the actual shape and all form factors will for small q develop universally into the same q-dependence. The radius of gyration expresses the 'typical size' of any finite-sized object, and is commonly used for particles, but also for polymer coils. The curvature at the upper limit of the scattering plateau gives thus direct access to the typical

size of the particles. Note that a another popular small angle extrapolation, the Zimm representation, which is a development similar to the Guinier one, yields identical results. Here, the inverse intensity is plotted and from $1/I = 1/I_0(1-(qR_g)^2/3)$ the slope yields the radius of gyration and the intercept with q=0 the forward scattering. This forward scattering is an extremely important parameter as it allows to access the volumetric information of the particle of which the scattering dependence is investigated. Still in Figure 1 but at large angles, finally, the scattered intensity is due to the surface between particle and 'matrix' and falls off rapidly, following a power-law envelope proportional to Aq^{-4} for sharp phase boundaries. This is called Porod scattering, and it is observed for well-defined interfaces. The prefactor A of the power-law can be directly related to the specific surface of the particles, S/V, a straightforward operation if the scattered intensity is known in absolute units:

$$A = 2\pi \Delta\rho^2 S/V \tag{6}$$

In the case of spheres, the specific surface can be easily calculated from the radius and volume fraction of spheres, $S/V = 3\ \Phi/R$, and vice versa. To summarize, the radius of monodisperse spheres can be determined from the low-q intensity, from the Guinier regime, and from the Porod decay. If these numbers agree, one may be quite sure of the spherical nature. If on the contrary they are in violent disagreement, there are different possibilities, namely deviations from sphericity, polydispersity, or both. An example for polydisperse spheres is also shown in Figure 1. The contribution of different ensemble averages to different parts of the intensity lead to an increase in the apparent particle volume (given by the low-angle limit, proportional to $\langle V^2\rangle/\langle V\rangle$, where $\langle\rangle$ denote the average over the size distribution), but it affects also R_g (its square is given by $\langle R^8\rangle/\langle R^6\rangle$), and the radius deduced from the Porod domain ($\langle R^3\rangle/\langle R^2\rangle$). Moreover, the oscillations of the form factor are almost completely wiped out by polydispersity.

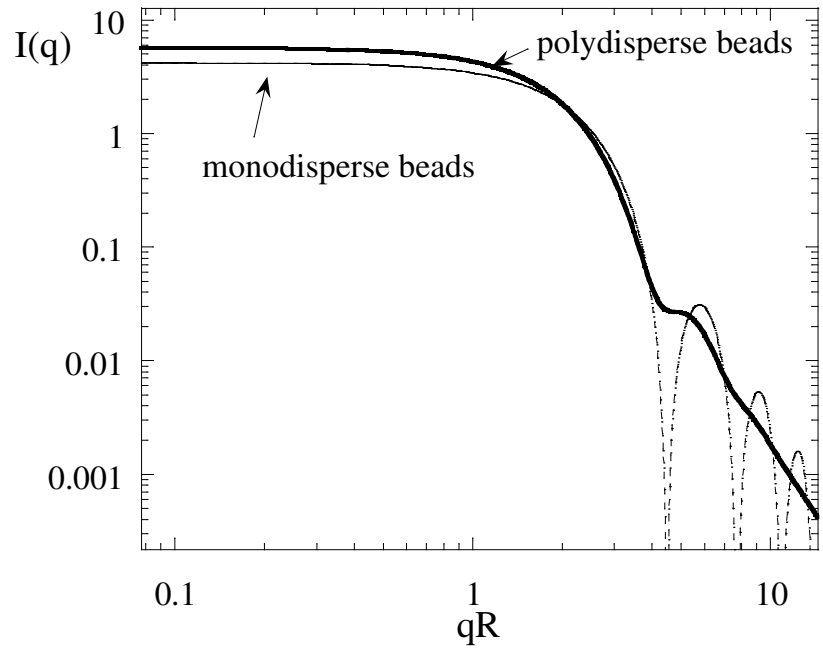

Figure 1: Example of form factor scattering of monodisperse and monodisperse spheres of identical contrast and volume fraction. Monodisperse (R = 100 Å), polydisperse (R_o = 100 Å, log-normal size distribution, σ = 0.15), plotted vs qR (resp. qR_o).

It is important to notice that different assemblies of particles can give very similar – in theory even identical – scattering. Polydisperse spheres and ellipsoids, e.g., may yield the same I(q). This is due to the loss of the phase information of the radiation when measuring its intensity instead of its amplitude. Fitting of scattering data will therefore never give a unique solution. One way out of this dilemma is cross-checking with other techniques, like direct imaging (TEM …). Another one is to concentrate on main features of the intensity, as outlined above: Average volume (low-q), average radius (intermediate-q), and average specific surface (high-q) are robust parameters measured without ambiguity. Combining them should already give a good hint on what the structure might be.

Another simple filler geometry is given by cylinders, which include rods and cylindrical platelets. Under dilute conditions, where the scattering is orientationally averaged and thus isotropic, the form factor of a cylinder of radius R_{cyl} and height (or length) 2 H reads [23]:

$$F_{cyl}^2(q) = \int_0^{\pi/2} \left(\frac{\sin(qH\cos\varphi)}{qH\cos\varphi} \right)^2 \left(\frac{2J_1(qR_{cyl}\sin\varphi)}{qR_{cyl}\sin\varphi} \right)^2 \sin\varphi d\varphi \qquad (7)$$

The introduction of an orientational distribution function in eq.(7) would be straightforward. In the case of stiff and long rods, H >> R_{cyl}, the scattering can be decomposed into a Guinier regime, intermediate and high-q scattering. At small angles, q < 1/H, one measures the radius of gyration and the cylinder volume if the concentration is low enough. In the intermediate regime, a power law decay in 1/q corresponding to one dimensional objects is observed, followed by the scattering reflecting the cross-section of the cylinder of area S. Using a Guinier approximation, this can be written in the intermediate and high-q domain:

$$I(q)=4\pi\Phi S\frac{\Delta\rho^2}{q}\left(\frac{J_1(qR_{cyl})}{qR_{cyl}}\right)^2 \underset{\text{Guinier}}{\approx} 4\pi\Phi S\frac{\Delta\rho^2}{q}\exp\left(-\frac{q^2R_{cyl}^2}{4}\right) \tag{8}$$

In the opposite limit of stiff and circular platelets, R_{cyl} >> H, the scattering can be described by an analogous Guinier regime at small angles, followed by the power law decay in $1/q^2$ characteristic of the 2D-platelet-structure. Together with the Guinier expression for the scattering in the direction of the height, the intensity reads (note that H is half the thickness):

$$I(q)=8\pi\Phi H\frac{\Delta\rho^2}{q^2}\frac{1-\cos(2qH)}{(2qH)^2} \underset{\text{Guinier}}{\approx} 4\pi\Phi H\frac{\Delta\rho^2}{q^2}\exp\left(-\frac{q^2H^2}{3}\right) \tag{9}$$

These particle morphologies are ideally suited to disperse in solvent or polymeric matrices and to yield new composite materials with new properties. Whereas several applications of composite solutions can be thought of, the major importance of blends of soft with hard matter is illustrated by the wealth of applications in daily life as tires and high-performance plastics. The soft polymers consist of more or less flexible chains of identical chemical groups, called monomers, which are connected into long arrays of a specific size, length and distribution, depending on the way how these long chains were prepared. The contour length of such a chain is L= Nl where l is the size of a monomer and N is their number. To exclude the influence of neighbouring segments which would affect the particular conformation of the monomeric groups, the chains can be re-partioned into Kuhn segments of length $l = C_\infty$ l and of number $N = N/C_\infty$. The numerical value for C_∞ goes roughly from 2 to 10 for the most common polymers. The larger C_∞ is, the stiffer is the polymer chain. This means that between two effective monomer (=Kuhn) lengths there is no correlation anymore and free rotation is assumed and allowed. This leads to a very similar situation as the random walk of a single

segment as all internal configurations have become equally possible and results of Brownian dynamics can be directly applied. The statistical independence of configurations in the chain is equivalent to a description with a Gauss distribution of internal distances which leads to the definition of the Gaussian chain. Several length scales in polymers can be defined. We refer to the broad literature for the specific details and only introduce here the necessary parameters to allow the understanding of the present review [11]. As polymers are statistical objects, one derives inherently averaged distances. The mean end-to-end distance of a polymer as determined from scattering experiments (scattering volumes of the order $0.1 cm^3$) is therefore the average over time as well as over a large ensemble of chains. It is found that $<R_{ee}^2>= Nl^2$ or likewise $C_{infty}\ Nl^2$. Small angle neutron scattering yields the Fourier transform of the pair correlation function which determines the so-called radius of gyration as introduced already in the section on particulates above. For a Gaussian random coil situation Debye could show that simply $R_g^2= <R_{ee}^2>/6$. The form factor of the chain is then calculated from

$$P_{gaussianchain=} = N^{-2} \sum_{i,j=1}^{N} \int dr_{ij} \exp(iqr_{ij}) p(r_{ij}) \tag{10}$$

where $p(r_{ij})$ is the Gaussian distribution. This sum leads to the simple expression in the second moments of the principal axes as

$$P(q) = N^{-2} \sum_{i,j=1}^{N} \exp(-1/2(q_x^2 < x_{ij}^2 > + q_y^2 < y_{ij}^2 > + q_z^2 < z_{ij}^2 >)) \tag{11}$$

The components of the scattering vector q are labeled x,y and z for generality and for all is valid in the isotropic state that $<x_{ij}^2>=<y_{ij}^2>=<z_{ij}^2>=<r_{ij}^2>/3$. With the definition of

$$R_g^2 = 1/2N^2 \sum_{i,j=1}^{N} < r_{ij}^2 > \tag{12}$$

the Debye chain form factor

$$P(q) = 2(\exp(-z) - 1 + z)/z^2 \tag{13}$$

with $z=(qR_g)^2$ is obtained. The decomposition of the form factor into its Cartesian components is a nice way to illustrate why polymers are ideally suited to probe on a microscopic level the outcome of macroscopic techniques and theories as is the case e.g. for the rubber elasticity. The reader may develop as an exercise the previous Guinier law for the polymer chain and will notice that smallest angle scattering is independent of the microscopic structure or shape of the scatterer. If a polymer is deformed into an anisotropic shape, however, the scattering of this shape will be anisotropic as well and will depend on the orientation of the sample with respect to the beam. The two-dimensional recording of the pattern therefore contains the stretching axis as well as one compressive direction, the other perpendicularly arranged being unexplored since it is scattering in beam direction due to the conservation of volume. Models of rubber elasticity can therefore be well probed by replacing the along strain $<z_{ij}^2>$ components generically by $f(\lambda)$ $<z_{ij}^2>$ where the $f(\lambda)$ function may assume different forms depending on the assumption of network deformation. A combination of both principal axes and/or fully taking into account the orientational dependence will allow to accept or reject models. More complicated descriptions as this one are available and will be introduced later in this chapter. The properties of polymeric nanocomposites, i.e. changing the mechanical properties can therefore be investigated by measuring the chain deformation in the presence of the hard phase as a function of volume fraction and other parameters. At the same time, the deformation of the particulates can be analyzed and special experiments on certain samples can be planned in order to highlight either phase of the composite. One should stress that only the SANS method, with the assistance of SAXS methods is able to contribute to the molecular understanding of the reinforcement process, due to powerful contrast matching possibilities.

II.3 Structure factors in interacting systems

The reality of reinforced systems is usually restricted to relatively high concentrations. In this case, the filler particles are not dispersed independently, but are affected by their mutual positions. The scattering measured in interacting systems contains then two contributions. The first one is the particle form factor measured following eq.(3), which describes the basic scattering units. The second one is called the structure factor S(q) in colloidal science. This additional term reflects the positional correlations between particles. Indeed, it is nothing but the Fourier transform of the particle pair correlation function, and can be written in terms of the position r_i of N particles [26, 27]:

$$S(q) = 1 + \frac{2}{N} \sum_{i \neq j} \exp\left(iq\left(r_i - r_j\right)\right) \tag{14}$$

For anisotropic systems, the vectorial dependencies of S(q) need to be kept, whereas in isotropic system the exponential can be replaced by a sin x/x, with x = qΔr [28]. In the simplest case of monodisperse spheres, the resulting intensity is given by the product of form and structure factor, i.e. S(q) is multiplied to eq.(3) to give:

$$I(q) = \Phi \, \Delta\rho^2 \, V \, F^2(q) \, S(q) \tag{15}$$

In Figure 2 the influence of structure on the scattering is illustrated. In dilute systems, where the range of interaction between particles is smaller than the average distance, particles are not positionally correlated, like in a gas, and S(q) = 1. Only the particle form factor is measured.

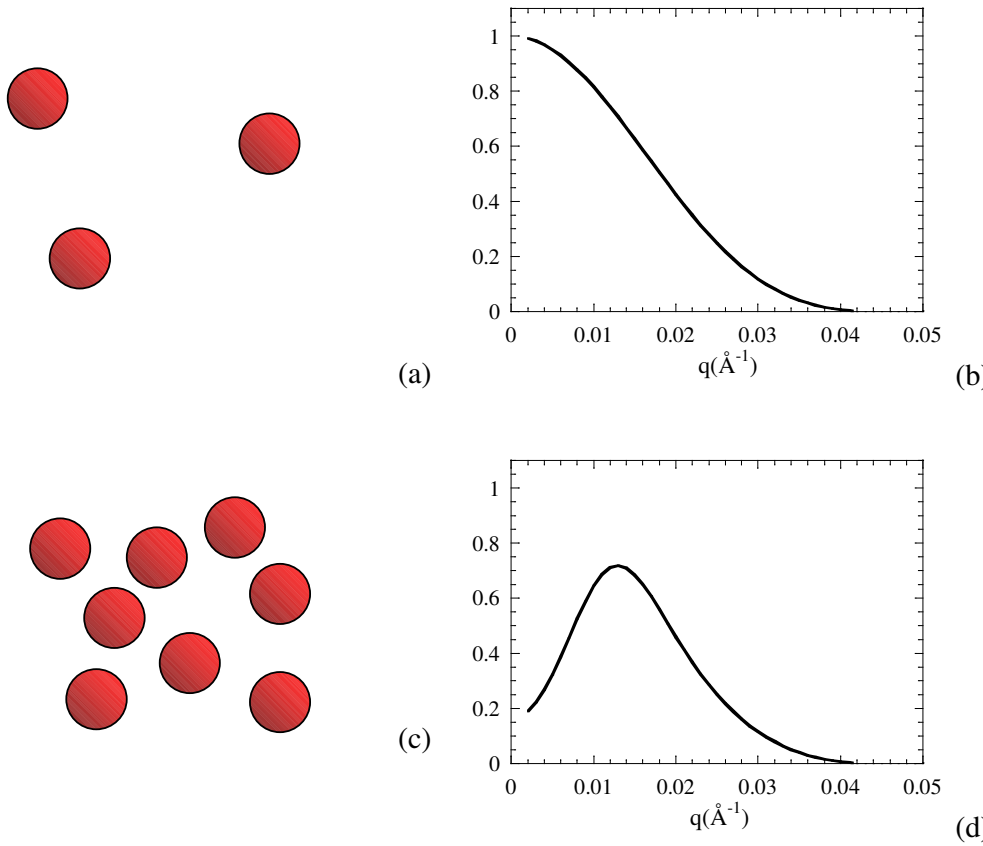

Figure 2: (a) Dilute and (c) interacting systems with the corresponding scattered intensity on the right (b,d). The cross-over from dilute to concentrated systems is roughly located where the average distance between particles is comparable to the interaction distance, e.g. the range of the pair interaction potential. In this model calculation we have increased the range when going from (b) to (d), at fixed concentration. Alternatively, we could also have increased the concentration at fixed range to generate the interaction peak, as suggested when going from (a) to (c).

At higher concentrations, S(q) deviates from one, and in the case of repulsive interactions depicted in Figure 2 the average distance between particles D becomes also the most probable distance. Then S(q) presents a peak at $q_o \approx 2\pi/D$.

As a last comment, one may note that it is good practice to measure if possible the form factor at high dilutions (S = 1), and obtain directly S(q) at higher filler concentrations using eq.(15) by division. The structure factor can then be compared to theoretical predictions. These can either be obtained quite easily by numerical simulation, or by use of published structure factors. The latter are usually derived from the Ornstein-Zernicke equation [26] with specific closure relations used for certain types of interparticle potentials. The simply analytical Percus-Yevick closures, e.g., is appropriate for short-scale repulsion, including hard sphere interactions [29], whereas the Rescaled Mean Spherical Approximation is good for long-range repulsion, including electrostatic interaction [30, 31]. Other closure relations are discussed in textbooks and reviews [26].

II.4 Aggregation of particles

Up to now we have discussed scattering from filler particles dispersed individually in a polymer matrix. Small colloidal particles are rarely in this state, and their aggregation is commonly encountered even in model systems. Here we discuss the scattering only in the simplest case of aggregation of monodisperse spherical particles. The description is not very sensitive to details, and can be generalized to slightly polydisperse systems, or anisotropic particles like clay platelets. We will the that the aggregation can be modelled by a term analogous to an intra-molecular term of large molecules.

As with well-dispersed systems, the filler volume fraction Φ is a key quantity both for structure and mechanical properties. Aggregates contain some matrix polymer, which can be shielded from the deformation, cf. the discussion of bound and occluded rubber in the introduction. This increases the effective filler volume fraction from Φ to Φ/Φ_A, where Φ_A is the volume fraction of filler inside an aggregate. The corresponding increase in size of aggregates pushes the system towards overlap, i.e. mechanically percolating paths of filler can be reached well below the close-packing of individually dispersed spheres.

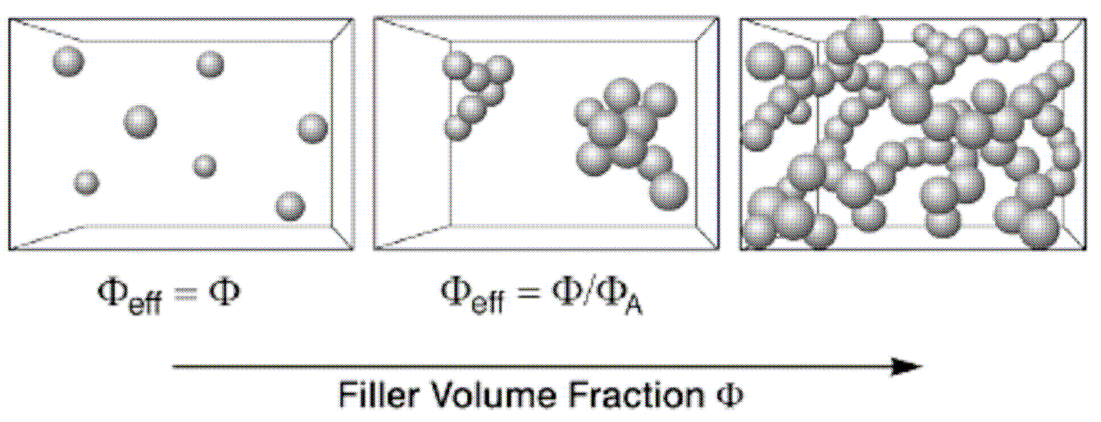

Figure 3: Schematic view of filler morphology in three concentration regimes. For Φ smaller than the overlap concentration Φ^*, reinforcement is due to hydrodynamic amplification by particles or clusters with $\Phi_{eff} = \Phi$ or $\Phi_{eff} = \Phi/\Phi_A$, respectively. For $\Phi > \Phi^*$ reinforcement is due to the deformation of a flexible filler network. Reproduced with kind permission of Springer Science and Business Media from ref. [32].

In Figure 3, we show an aggregated system below and above the overlap concentration Φ^*, above which the aggregates touch and interact. Below Φ^*, aggregates are dispersed and the mechanical properties are the ones of a dilute system. In this case, the scattering can be described by the form and structure factor formalism given above, with a the form factor of an aggregate given by:

$$P_{agg}(q) = \left[1 + \frac{2}{N_{agg}} \sum_{i \neq j}^{N_{agg}} \exp\left(iq\left(r_i - r_j\right)\right)\right] P(q) = S_{intra}(q) P(q) \qquad (16)$$

where the sum extends over the positions of the N_{agg} particles (of form factor P(q)) inside one aggregate. It can be guessed directly from eq.(16) that the forward scattering $I(q \rightarrow 0)$ is increased by a factor N_{agg}, where N_{agg} is the number of particles in an aggregate. This increase is used, e.g. with light-scattering, where q is very small compared to the inverse particle size. The aggregation of dilute colloidal systems in solvents can thus be followed directly via $I(q \rightarrow 0)$. At intermediate q, the scattering function calculated using eq.(16) decreases following a Guinier law, eq.(5), with the radius now being the aggregate radius of gyration instead of the particle one. At higher q values, S_{intra} presents a minimum followed by a maximum. The latter is due to the interparticle correlations, and the position of the maximum reflects the average center-to-center distance between neighbouring particles, i.e. $q = 2\pi/2R$

for close packing. The height and sharpness of the maximum gives information on the relative occurrence of close spheres, in other words on the first coordination number. Intra-aggregate structure factors are discussed for model aggregates constructed by computer simulation in [33, 34], and an example is shown in Figure 4. A special case is given by tactoids in clay-polymer nanocomposites. In such finite stacks of lamellae the aggregation is one dimensional, with the typical distance D and the corresponding peak at $q = 2\pi/D$ [35].

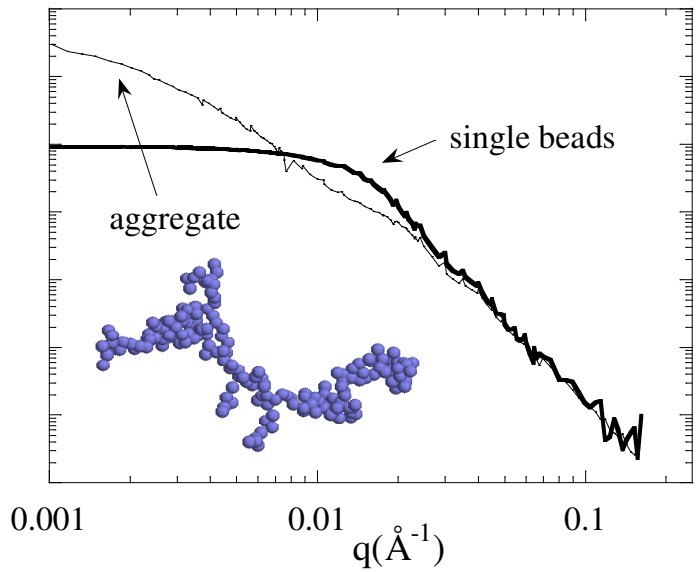

Figure 4: Form factor of simulated aggregate and form factor of individual beads under identical volume fraction and contrast conditions. The low-q increase is related to the increase in mass, the intermediate scattering is determined by the aggregate statistics, and the high-q scattering is of course due to the surface scattering, identical in the two cases.

Concerning aggregate structures, two cases are typically encountered. First, aggregates can be homogeneous, e.g. dense assemblies of spheres. In this case their density does not depend on their size, and may be given, e.g., by the close packing volume fraction (e.g. refs. [36, 37]). The second important family of aggregates are fractal aggregates. For such aggregates, the density decreases with size, and the number of particles N_{agg} in a fractal of size R is given by

$$N_{agg} = (R_{agg}/R)^{Df} \tag{17}$$

with R the primary particle radius and D_f the fractal dimension. There is huge literature on fractal growth processes and structures, and the reader is referred to it for an in-depth discussion of the different growth scenarios, and the fractal dimensions associated with them

[38]. The scattering from isolated fractals can be described by the same eq.(16) as before, all the information being hidden in the mutual positions of particles used to evaluate the sum. For finite-sized fractals, which means for scattering that they are small enough to enter the q-range of observation, the scattered intensity starts as in the discussion above from the forward scattering proportional to N_{agg}, followed by a Guinier regime. The difference with homogeneous particles is the existence of an intermediate scattering regime, where I(q) follows a simple power law [39]:

$$I(q) = \frac{B}{q^{D_f}} \quad (1/R_{agg} < q < 1/R) \tag{18}$$

In the literature, several calculations of the complete scattering function exist, especially with the finite-size described by the crossover to the Guinier regime at $1/R_{agg}$, and the particle scattering taken into account by the crossover to a particle form factor [40-42]. These will be discussed in the corresponding sections together with the experimental results.

Finally, above Φ*, aggregates interact, and depending on the system under investigation, this can lead to different situations, the scattering of which may be difficult to model. Aggregates might, e.g., interpenetrate, or undergo internal reorganizations. In analogy with the transition from dilute to semidilute regime of polymer solutions [43], Φ* depends on the space filling properties of the aggregates. Unfortunately, no general description exists in the case of interacting aggregates, and one must construct appropriate models for each case. This was done successfully, e.g., by combining standard theory of liquids with aggregate form factors in a silica-latex system [44].

III. Structure of chains in polymer nanocomposites

Polymer-filler systems are complicated and structured multi-component as well as multi-phase systems. Extracting the information of interest from scattering results, demands sophisticated labelling techniques as well as a suitable theoretical treatment. If the chain scattering is to be resolved, the full intensity has to modelled.

III.1 General expressions for chain scattering in multi-component systems

The total differential cross section $d\sigma/d\Omega$, which is proportional to the measured intensity ($d\sigma/d\Omega = V_s\, d\Sigma/d\Omega$, V_s being the scattering volume), can be expressed in terms of the partial structure factors for a general nanocomposite system:

$$\frac{d\sigma}{d\Omega} = \sum_{I,J} b_I b_J S_{IJ} \tag{19a}$$

with the partial structure factors

$$S_{IJ} = \sum_{ij} \left\langle \exp\left[-i\vec{q}\left(r_i - r_j\right)\right] \right\rangle \tag{19b}$$

where the index 'i' runs over all scattering entities (atoms, molecules) belonging to the component I (i.e. one type of particles, the matrix, …), and similarly for j (J). The partial structure factors are thus nothing but a part of the general sum of interferences building up the total intensity. It may be noted that the intensity can also be directly transformed into a sum of correlation functions of the scattering length density. The game is therefore to play with the contrasts, i.e. the prefactors b_i in eq.(19a) in order to switch off or on certain contributions, or correlation functions. As an example, the scattering from a particulate consisting of two scattering components, like a core and a shell, and the matrix designed to allow the single chain extraction via a H/D labelling of the chains, can be expressed then by four diagonal (intra-component) and six off-diagonal (inter-component) partial structure factors :

$$\begin{aligned} \frac{d\sigma}{d\Omega} &= b_1^2 S_{11} + b_2^2 S_{22} + b_3^2 S_{33} + b_4^2 S_{44} \\ &+ 2b_1 b_2 S_{12} + 2b_1 b_3 S_{13} + 2b_1 b_4 S_{14} + 2b_2 b_3 S_{23} + 2b_2 b_4 S_{24} + 2b_3 b_4 S_{34} \end{aligned} \tag{19c}$$

The scattering properties can be expressed conveniently for two- and three-component systems in terms of the intra-component structure factors only. The simplest case, i.e. treating a polymer-filler (p-f) system as a two-component filler-matrix system is obtained with $S_{11} = S_{ff}$, $S_{33} = S_{pp}$, $b_1 = b_f$, $b_3 = b_p$, $b_2 = 0$, $S_{33}=S_{13}=S_{23}=0$, the incompressibility condition leads to the well known relationship

$$S_{ff} = S_{pp} = -S_{fp} \tag{20}$$

of the intra- (S_{ff} and S_{pp}) and the filler-polymer contributions S_{fp} . Then for the differential cross section follows in analogy to the two component system

$$\frac{d\sigma}{d\Omega} = \left(b_f - b_p\right)^2 S_{ff}\,(\mathrm{q}) \tag{21}$$

For four-component systems such a presentation is not possible and the general form is needed, requiring several experiments to allow all unknowns to be eliminated. It can be shown that simple contrast matching is not possible anymore and two different conditions, e.g. matching either core or shell in case of a core-shell filler, emerge from it. Sometimes, such a system can be reduced to an effective three-component system which most of the time is a good approximation with regard to the size of the heterogeneity. The total structure factor is then simply obtained as

$$\frac{d\sigma}{d\Omega} = \left(b_{<f>} - b_{<p>}\right)^2 S_{ff} + \Phi_p \left(b_H - b_D\right)^2 S_{RPA,p} \tag{22}$$

where p and f stand again for polymer and filler, and brackets < > denote averaging over the particular phase. If the nanocomposite phase can be matched against a polymer blend of H and D chains, the first term disappears and the chain scattering becomes available. On the other hand, if the polymeric phase is not labelled, the second term is not present and the former treatment becomes apparent, simulating the SAXS investigation with a different contrast factor. The structure factor of the elastomeric phase is the well-known RPA structure factor and is weighed with the volume fraction of the polymeric phase. Details of the lengthy derivation can be found in our former work [45, 46]. The derived structure factor shows at least that the total cross-section can be expressed by the structure factor of the filler, i.e. the domain scattering and by the structure factor of the chains inside the polymer matrix. From the first term it can be easily seen that by a suitable choice of the scattering lengths of the components an extinction of the phase scattering should be in general possible even in the case of an heterogeneously composed filler. The result is general and applicable to both neutrons and X-ray investigations. Latter will always lead to the first component, former may have both.

The labelled polymers are assumed to be randomly distributed over the polymeric phase and no preferential interactions between the filler and the components of the polymer matrix are assumed, irrespective of the fact that the filler surface may be fractal. S_{RPA} contains the intra-chain structure factors of the polymer chains.

The same scattering theory can be generalized also to include the effect of strain. S_{ff} and $S_{RPA,p}$ can be taken dependent on deformation and the polymer scattering interpreted in terms of the tube model for entangled polymers [11]. The structure factor of a single chain with N monomer segments subjected to tube confinement *without* extra restrictions due to crosslinking points is then written as

$$S(\vec{q},\lambda) = 2N\int_0^1 dx\int_0^x dx'\prod_\mu \exp\left\{-(Q_\mu\lambda_\mu)^2(x-x') - Q_\mu^2(1-\lambda_\mu^2)\frac{d_\mu^2}{2\sqrt{6}R_g^2}\left(1-\exp\left[-\frac{(x-x')}{\frac{d_\mu^2}{2\sqrt{6}R_g^2}}\right]\right)\right\} \tag{23}$$

$Q_\mu = q_\mu R_g$ is the component of the reduced scattering wave vector in the main axes system of the deformation tensor, d_μ the (anisotropic) tube diameter, and λ_μ is the microscopic deformation in the same main axes system. The variables x and x′ are dimensionless contour length coordinates extending over the considered labelled paths. The first term in the exponent corresponds to the scattering of an affinely deformed Gaussian chain with radius of gyration R_g, whereas the second term accounts for the non-affine contributions due to chain fluctuations. The tube concept is a mean-field approach, which takes into account the natural restrictions on the configurations on the chains due to the uncrossability of chains. It is considered to be a very good approximation if the restrictions are strong Then the control parameter $\frac{d_\mu^2}{2\sqrt{6}R_g^2}$ is only a small quantity and contributions of the second term in the exponent come from very short parts of the chain only. This leads to a nearly affine behaviour of $S(\vec{q},\lambda)$ up to the largest scattering vectors which are attainable in SANS. This treatment contrasts the simple decomposition in cartesian components before as there no

interaction between chains was allowed, a result immediately related to the random walk statistics of polymers which is equivalent to fully interpenetrating volume-less and interaction-less chains.

The result for single (i.e. dilute) labelled paths, can be extended to interacting (i.e. concentrated) systems. Then the RPA results consider the restrictions on interchain correlations due to the low compressibility of dense polymer systems [46]. It takes the form

$$S_{RPA,p}(q,\lambda_m) = S_{0,RPA,p}(q,\lambda_m) * S_{WE}(q,\lambda) / S_{Debye}(q,\lambda\ ) \tag{24}$$

The subscript '0' refers to pure affine deformation with λ_m , given as in eq. (23) and WE and Debye stand for the Warner-Edwards tube model and isotropic Debye curve scattering [47]. The quotient of the latter yields the fluctuation contribution on top of a deformed interacting blend. Inter- and intra correlations, i.e. RPA and segmental fluctuations are treated separately.

The final aim of such investigations will be the determination of chain deformations as well as of the filler components. If additivity of phase and chain scattering is given, however, a sufficiently precise knowledge of the q-dependence of the phase scattering is still necessary. Former can be done rigorously without knowledge of the filler structure if complete matching of the domain scattering is achievable. On the other hand, this q-dependence can be obtained by investigating identical samples both with simple protonated polymer matrix. But because this matching approach cannot be realized without uncontrollable uncertainties, the approach to combine SANS and SAXS measurements on the same sample works much better and allows also the correction of SANS spectra for eventual contribution from the filler structures. In following the results for both systems are summarized. To be general, the filler scattering which is not treated here, was modelled -where necessary- by the hierarchical Beaucage model [41, 48].

III.2 Chain structure in multi-component systems

The study of reinforcement or in general that of composite materials and its implications for the final properties is directly linked to the quality of describing macroscopic properties as the dynamic modulus or simple stress-strain curves. To ‘understand’ the obtained curves, a model

is always necessary for which ideally the parameters can be chosen on the basis of microscopic details. This means practically crosslink densities, strain measures and the consideration of the appropriate fluctuations. These three most simple parameters have already split the network classes into affine, phantom and constrained chain/junction networks, each determined by different strains and fluctuations. The most complete theoretical model, however, which unifies them is still the tube model for which also several versions are available [11]. However, as said before, it is virtually only due to the SANS technique that the models could be validated against macroscopic experiments as all needed geometric information is contained naturally in the scattering. It is therefore a natural extension that also this method should be considered in the nanocomposite field. This means inevitably multicomponent treatment which gets very complicated for more than three different contrasts, IF one is to investigate the soft matrix.

In this context, the terminology of composition matching and phase matching has become popular. Obviously a thermodynamically homogeneous phase like the polymer matrix can contain labelled chains, i.e. have a non uniform composition. If the scattering is chosen such that the scattered intensity is due to the difference between two phases (e.g., matrix and filler), independent of composition, the scattering of a phase (e.g., the filler) is observed. It allows the form and structure factor of a component of the composite to be determined. If however, the average compositions of the phases are arranged in such a way (e.g. by introducing D-labelled chains in the matrix) that the structure hard-soft does not produce scattering length density variations, the system has composition matching, and only density fluctuations within each phase contribute to the scattering. This is the case where, e.g., chain structure within the matrix can be observed.

Given the possible complexity, physical systems can be subdivided in different classes: (i) Two-component, two-phase with homogeneous scattering length density within the phases. This case corresponds as well to amorphous polymers filled with homogeneous filler as also to a blend of immiscible polymers. (ii) Two-component, one phase. This is the case of a blend of miscible polymers (e.g. a blend of deuterated and "normal" H-containing macromolecules) which can be described by the famous RPA-approach. (iii) Three component, two phase with the filler as one phase and a miscible polymer blend as second phase. (iv) Four component, two phase with the filler considered as one phase but e.g. a more complex core-shell structure with different scattering properties and a polymer blend as second phase.

Here we summarize the approaches that were made without going into details. Quan and Koberstein in 1987 first derived a method to observe polymer chain scattering in a three-component two-phase composite, based on the contrast variation technique [49, 50]. The method is an extension of the well-known contrast variation method with solvents in which a solvent mixture is used to match out a component. Similar results are therefore obtained by Williams et al and Ackasu et al [51, 52]. These approaches have been used typically for investigation of three-component problems based on polymers, i.e. mixtures of block copolymers and linear homopolymers which are part of a specific phase or morphology [53].

Recently this approach was applied also by Nakatani for silica-filled PDMS composite blends, which were 'filled' by a sol-gel process [54, 55]. The approach lacks generality in that it is applicable for chains of different molecular weights and also interchain interactions are neglected. Further it assumes a homogeneous third component. Two years earlier, Westermann et al used the same approach for polymeric fillers, which were created by microphase separation of PS segments of a PI-PS-PI triblock in a PI homopolymer environment [56]. Their work is the first one on crosslinked networks and in which the phase- and composition matching was almost perfect. The hydrodynamic effect that the particles exert on the chain, i.e. increase the strain in the soft matrix, could be proven unambiguously and for the first time also empirical laws of reinforcement could be validated. This particular investigation made the bridge between the normal unfilled rubbers and filled rubbers and allowed predictions of the tube model for composite materials to be tested. The analysis of the deformed composite network was done using both neutron and X-ray small angle scattering and only by this combination the interesting link to mechanical measurements was possible. The success of this approach for composites has lead to further work of this group into silica-rubbers composites. To get rid of the limitations of Nakatani e.g. - i.e. solvent-like treatment, simple composite, no strain-model if deformed and neglect of chain interactions - Botti et al presented a new way to extract the chain scattering from a two-phase four-component structure with the RPA method, which can be simplified [45]. In the strained state, it was possible to distinguish even between strain effects on the filler related to the Mullins effect as well as on the rubbery chain network. Unlike for the polymeric filler, it showed that contrast matching of the phase is nearly impossible due to inevitable heterogeneities in the filler like surface modifications and density variations. The authors deal with these problems using either direct subtraction of X-ray data in the isotropic case or by reducing the anisotropic

difficulties by combining uniaxial and compressed strain direction intensities [46]. No further literature on chain scattering with composite character are known to date, besides a recent contribution by Sen et al on chain conformations in polystyrene loaded with silica particles [57]. These authors show that in their system chain radii of gyration are not modified by the addition of silica, even though some experimental difficulties related to the exact matching of the silica remain. To summarize this subsection, given the importance of nanocomposites for enhanced mechanical properties, many new aspects can be expected for the description of chain deformation and dynamics.

IV. Structure of filler in polymer nanocomposites

We will now review studies of the structure of filler particles in polymer nanocomposites as seen by scattering experiments. The analysis of the published scattering data is not always an easy task, due to the complexity of the systems. However, we will see that the basic tools given in the introduction can be used to extract useful information, especially in simple systems. In more demanding cases, two complementary theoretical tools have been proposed, fractal models and reverse Monte Carlo (RMC). We will discuss applications of both in this section. Finally, note that contrast variation methods have been shown to be quite powerful, but will not be discussed here [58].

In order to emphasize the importance of structure, we start with a perfect illustration of the influence of structure on the mechanical properties published by Pu et al [59]. The only drawback of this work is that it does not have anything to do with scattering, but it serves our purposes quite nicely. Pu et al have used electron microscopy to characterize the state of dispersion of silica particles in poly(methyl acrylate) elastomers. In Figures 5a to 5c, randomly dispersed, ordered and aggregated filler particles are easily seen. These samples have been made by either mixing the silica particles with the monomer for polymerization (random dispersion), or by mixing them but wait before the polymerization (ordered), or at last by drying them before mixing them with the monomer (aggregates). In the article by Pu et al, the stress-strain isotherms of 45%-silica samples are compared. At small deformations, the behaviour is quite similar. At larger deformations, the ordered and randomly dispersed nanocomposites break, whereas the aggregated one breaks at a comparable stress, but much later. The toughness, which is measured by the integral under the stress-strain curve, is thus much higher in the aggregated case. Although the influence of aggregation is not always

comparable from one system to the next, this example demonstrates the effect of structure on the mechanical properties.

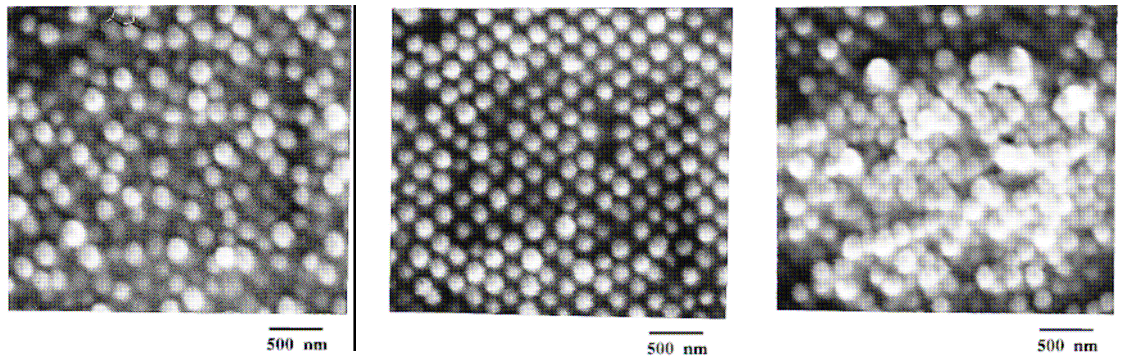

Figure 5: Electron microscopy results obtained by Pu et al of sample containing 40%wt of silica (a) randomly dispersed, (b) ordered, and (c) aggregated. Reproduced with permission from ref. [59]. Copyright (1997) American Chemical Society.

This section is divided into three parts, which correspond to two important classes of filler particles, carbon black and silica, whereas the third section is dedicated to clay and polymeric filler, where scattering has been used much less. It is recalled that a general review of current literature on the different types of fillers used for polymer nanocomposites has been published by Schmidt and Malwitz recently [6], and that reviews on filler structure [7] and reinforcement theories are available [3]. In the first part of this section, we will review the structure of carbon black. Carbon black has considerable structural complexity, the different levels of which can be nicely seen in scattering experiments, and conveniently described by a model by Beaucage [41]. The structure before and after incorporation into a polymer matrix will be discussed. It has been shown by theoretical studies, and in particular by Witten et al [8, 60, 61], that the rigidity of a carbon black aggregate decreases very quickly with size. This explains that under the strong shear usually necessary to incorporate carbon black powder in the melt, aggregates break up down to a characteristic size, which can then be analysed by scattering studies of nanocomposites.

In the second section, we turn to the structure of silica in polymer matrices. Poly(dimethyl siloxane) and other siloxanes are commonly filled with ‘high structure’ particulate silica in order to improve mechanical properties, as PDMS does not have any self-reinforcing

mechanism like strain crystallization. Of course the natural compatibility between silica and silicones is an important parameter in the choice of the filler, and the resulting reinforced elastomers are know for their good optical transparency. As with carbon black, there are different ways to blend the filler with the polymer. The incorporation into a high-viscosity polymer being both time-consuming and energy-intensive, several sol-gel routes have been developed, among which the generation of filler during curing which allows to circumvent difficulties with mixing [62]. In this second section, we will review combined scattering and mechanical studies, and also present a structural model based on Monte Carlo simulations, called Reverse Monte Carlo [63]. It allows the description of the three dimensional structure of the nanocomposites in filled systems with strong interaction between filler particles.

In the last section, scattering studies of fillers different from the two main types, silica and carbon black, will be discussed. This includes mainly clay and polymeric fillers, i.e. very popular domains, but where only few articles with fundamental progress in the interpretation of complex scattering data have been published.

IV.1 Structure of carbon black

Both historically and economically, carbon blacks are the most important filler particles used for reinforcement of rubber. They are produced in many grades, depending on the required performance of the final product. For reinforcement purposes, thermal and furnace blacks, produced by incomplete combustion of hydrocarbon gases or oil, are usually employed.

Their generic structure is produced by a random aggregation of primary particles, which are bonded by sinter bridges [32]. The resulting aggregates are rigid, of typical size 50-100 nm, and have a ramified or fractal structure. They infer different properties to an elastomeric matrix, depending on the size of the primary particles, and the structure and the specific surface of the aggregates. The aggregate structure is usually characterized by electronic microscopy and adsorption isotherms [64], in particular oil (dibutyl phthalate, DBP) adsorption. As with any adsorption process, the size and properties of the probe molecule are important, and the adsorbed amount is characteristic of the voids and surface available to a specific molecule. For DBP, typical values are of the order of 1 cm^3 per g, a value which is taken as synonymous of the structure of the carbon black. Again, we underline that this differs from the “structure” we are interested in here, i.e. the spatial arrangements of the primary

particles inside aggregates after incorporation in a polymer matrix. Note that the incorporation is a process which may also modify the carbon black structure, e.g. through shear [32]. We will now review several studies of the structure of carbon blacks with scattering techniques. We will see that scattering allows for a precise description of the average structure, in polymer matrices, suspended in solvents, or in the pure state.

The structure of pure carbon blacks as seen by SAXS has been discussed in a recent article by Rieker et al [65], and we use this work as a representative example for a larger body of work. These authors have studied nine different commercial carbon blacks which were collected before pelletization in order to preserve their initial mass fractal character. In their data, the different levels of organization of the carbon blacks can be easily identified. At very small angles, the authors invoke large agglomerates of carbon black aggregates. The first power law, with slopes between –1.5 and –1.9, corresponds to the mass fractal organization of aggregates. These values are in the same range as the mass-fractal dimension expected for diffusion-limited carbon cluster aggregation, 1.78. This power-law behaviour crosses over to the Porod regime, with an exponent of –3.8, i.e. close to 4. At very large angles, finally, there might be some evidence for scattering from graphite sheets, with an exponent of –2. This point has lead to some discussion in the literature ([66], and refs. therein), namely concerning the interpretation of deviations from the Porod law. Hoinkis et al conclude that the surface of Corax N330 carbon black was essentially smooth on length scales of 1 to 5 nm, although the high-q scattering did not follow a Porod law [66]. Coming back to the work by Rieker, the carbon black grades selected by the authors seem to have a very similar structure [65]. This is partly due to the presentation on log-scale, where factor-of-two shifts in the position of the break in slope are not easily seen. In their conclusion, the authors address the question of the influence of polydispersity on the position of the break in slope of I(q). In particular, they show that the high polydispersity in primary particle size (as measured by direct imaging with TEM) does not allow the quantitative determination of the average size from the break in slope. On the other hand, it is clear that for sufficiently monodisperse primary particles the break in slope can be described by Guinier-scattering, cf. eq.(5), which gives a good estimation of the particle diameter. We will come back in the next section to the complete modelling of the data, using Beaucage's expression.

IV.2 Structure of carbon black in polymer nanocomposites

The mechanical properties of polymer can be reinforced by the addition of carbon black, and indeed carbon black is one of the most important fillers for car tires. In this particular application, the reinforcement of the rubber aims at the optimization of many, sometimes contradictory functions, including load-carrying capacity, dampening, minimum noise and vibrations, transmission of driving and breaking torques, resistance to abrasion and low rolling resistance [1]. The reinforcement effect is closely related to two different aspects of the filler, interfacial properties [67] and aggregate structure [3, 68]. The chemical properties of the interface and the specific surface determine the compatibility between the matrix and the filler, with the extreme case of chemical bonding. If we keep this parameter fixed, then the influence of the structure can be studied. The influence of the fractal structure on the mechanical properties has been discussed by several authors [8, 68], and we concentrate on the measurement of these structures by small angle scattering.

In the mid 90s, Beaucage has developed a structural model describing the intensity scattered by independent (i.e., under dilute conditions) fractals from the Guinier regime, eq.(5), into the intermediate scattering, eq.(18) [41]. Similar approaches had been published by Sinha [42], as well as by Teixeira [40]. The Beaucage equation, which can be looked at as a convenient unified expression of the Guinier and the fractal scattering, reads:

$$I(q)=G_1\cdot\exp\left(-\frac{q^2R_g^2}{3}\right)+B_1\cdot\left\{\frac{\left[\mathrm{erf}\left(qR_g/6^{1/2}\right)\right]^3}{q}\right\}^{D_f} \qquad (25)$$

The second term corresponds to the fractal structure of the aggregate, the error function allowing for a smooth cross-over. Amongs its advantages one may cite that this equation can be easily extended to several levels [41, 69]. If we introduce a second level, which can represent the scattering of the primary particles, Beaucage's expression reads:

$$I(q)=G_1\cdot\exp\left(-\frac{q^2R_g^2}{3}\right)+B_1\cdot\left\{\frac{\left[\mathrm{erf}\left(qR_g/6^{1/2}\right)\right]^3}{q}\right\}^{D_f}\cdot\exp\left(-\frac{q^2R^2}{3}\right)$$
$$+G_2\cdot\exp\left(-\frac{q^2R^2}{3}\right)+B_2\cdot\left\{\frac{\left[\mathrm{erf}\left(qR/6^{1/2}\right)\right]^3}{q}\right\}^{p} \qquad (26)$$

Now the fractal law is weighted by the Guinier expression of the second level, which is the scattering of the primary silica particle in our case; this effectively suppresses the fractal law of the first level at high q. This is followed by an equivalent expression of the higher level, i.e. a Guinier law of primary particles followed by the power-law, which can be the Porod law of the primary particles if we set p=4.

In a recent article, Beaucage et al study the morphology of polyethylene - conductive carbon black composites by SAXS [70]. As we have outlined above, carbon black is organized on different length scales. The analysis of data that contain multiple level of superimposed structure is made possible by the use of the unified equation, eq.(25). In the case of a two-level structure, there is a crossover in I(q) between the first power law ($1/q^{Df}$) to the second one, which is usually the particle scattering. If the particles are monodisperse and have well-defined interfaces, then they have Porod scattering with p = 4. If the surfaces have themselves a fractal structure, then the high-q scattering is proportional to $1/q^{6-Ds}$, where D_s is the surface fractal dimension. In their paper, the authors discuss the effect of polydispersity on the scattering from aggregates. In particular, they show that even in the absence of particles with a self-similar surface roughness, an exponent different from 4 over a given q-range can be generated by a wide polydispersity in size, e.g. a power-law distribution. In simple terms, the addition of particle scattering from particles of different sizes, each with its own crossover from Guinier to q^{-4} scattering, can create a powerlaw scattering profile with an exponent different from 4.

In the experimental part of the article, Beaucage et al analyse the morphology of carbon black – polyethylene samples, which were high density poly(ethylene) (HDPE) containing 5%v of commercially available furnace carbon black of nominal diameter 800 Å [70]. This type of carbon black is conducting, which explains the application the authors were interested in, circuit protection devices. When heated through a strong courant, the conducting phase and the matrix reorganise, decreasing carbon black percolation and thus conductivity [71]. The

structural evolution with thermal treatment was followed in this reference, but here we concentrate on the structure analysis itself. The scattering experiments were performed on compression-molded plaques of approximate thickness 0.25 mm, after milling of the polymer and carbon blends. At small angles and low concentrations, the resulting scattered intensities did not show any signatures of concentration effects, i.e. there was no need to take aggregate-aggregate structure factors into account. As can be seen in Figure 6, there is a small Guinier domain at small angles, corresponding to an aggregate size of 1580 Å. At higher concentrations (35%), this size decreased, which suggests some cut-off mechanisms due to mixing. The Guinier domain is followed by a power law with an exponent of –3.59. A priori, such a high value suggests scattering from a surface-fractal, with a surface fractal dimension of 2.41, as mass fractal would have an exponent less than 3. Electron microscopy of this carbon black, however, does not show any significant surface roughness. The authors then point out that there is a numerical relationship between the high-q power law exponent close to –3.6 and the heterogeneity index HI. This index is a measure for polydispersity in aggregate size, an is obtained through microscopical observations. Most furnace blacks have a power law exponent close to –3.6, and a HI of about 2. Beaucage et al show that a power law polydispersity simultaneously explains both the HI and the exponent of the intensity decay.

Upon a closer look on the data, several deviations from this ideal scattering behaviour are identified. In HDPE, the intensity at intermediate angles is polluted by the scattering from the PE-crystallites. For comparison, experiments on the same carbon black incorporated in amorphous polymer PMMA were performed. In this data, there is a slight hump in the intermediate q-range, which has been described by the authors through the introduction of a second size level. It corresponds roughly to primary particles. Their size is found to be smaller (200 Å) but of the same order of magnitude than the nominal value. In their paper, the authors discuss possible sources for this discrepancy, which might be due to the internal structure of the primary beads, or to the measurement by different methods of different moments of the same size distribution. At large angles, finally, the carbon black substructure becomes visible, as there is the q^{-2} scattering of graphitic layers.

In conclusion, the authors have shown that it is possible to quantitatively characterize carbon black polymer nanocomposites by means of small angle scattering. Using the unified Beaucage equation, they are able to extract information on a complex system, where

microscopy is limited by overlap of structural features in three dimensions, and the simultaneous spatial organization on different length scales.

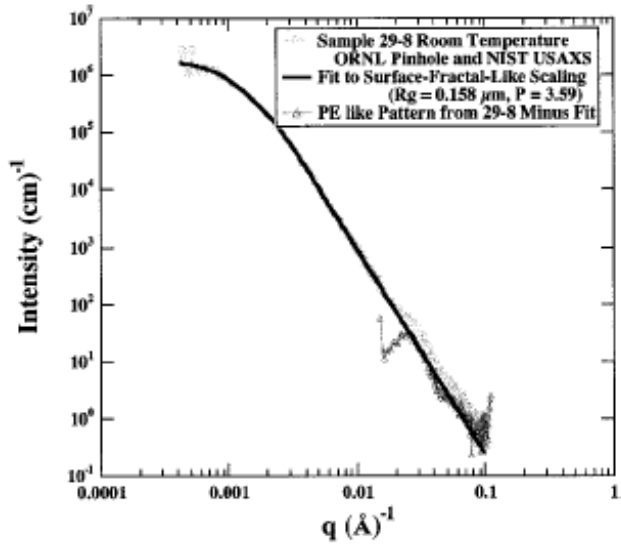

Figure 6: Typical USAXS and SAXS data from a carbon black – PE composite of 5%v. The fit has been obtained at low q using eqs. (25) and (26), with a power-law exponent of 3.59. There is a slight difference at high q, which can be explained by scattering of PE of similar crystallinity. Reproduced with permission from ref. [70].

One of the many advantages of scattering studies is that they can be performed with anisotropic samples. Indeed, if the beam collimation is symmetric in the x and y direction, i.e. the lateral resolution is identical or at least comparable in the two directions perpendicular to the beam direction, then a two-dimensional detector allows the characterization for instance of stretched polymer nanocomposites, an example of which will be discussed now.

Belina et al have performed SAXS and SANS experiments in order to elucidate the microscopic structure of filler particles in filled industrial rubber [72]. Their samples contain additives, among which is ZnO needed for the vulcanization. The electron density of ZnO is very high compared to that of carbon, which partially compensates its low concentration in SAXS experiments. In order to isolate the carbon black scattering, it was therefore necessary to do SANS experiments. Indeed, the neutron scattering length density of ZnO being comparable to the one of carbon, the huge difference in concentration made the scattering of ZnO negligible. The authors demonstrate this by comparing SANS and SAXS experiments, and conclude that the SAXS data are dominated by the ZnO signal. They then analyze an anisotropic scattering pattern obtained with a sample stretched to $\lambda = 2.5$, cf. Figure 7. The

pattern is a very characteristic 'butterfly' pattern [73], which is usually associated with inhomogeneous deformation in the range of the length scale corresponding to the peak intensity, i.e. in their case about 200 Å. The data is then analyzed with Beaucage's model, eqs.(25) and (26), along the stretching direction, and perpendicular to it. It is found that the aggregates have a comparable size of approximately 200 Å of radius of gyration, but quite different fractal dimensions in the two directions. Parallel to the stretching, $D_f = 1.8$ is found, which corresponds to the fractal dimension of unperturbed carbon blacks obtained by cluster aggregation. Perpendicular to it, D_f is much lower, close to 1. This difference in fractal dimension if reflected by the butterfly pattern, and we will come back to its interpretation shortly.

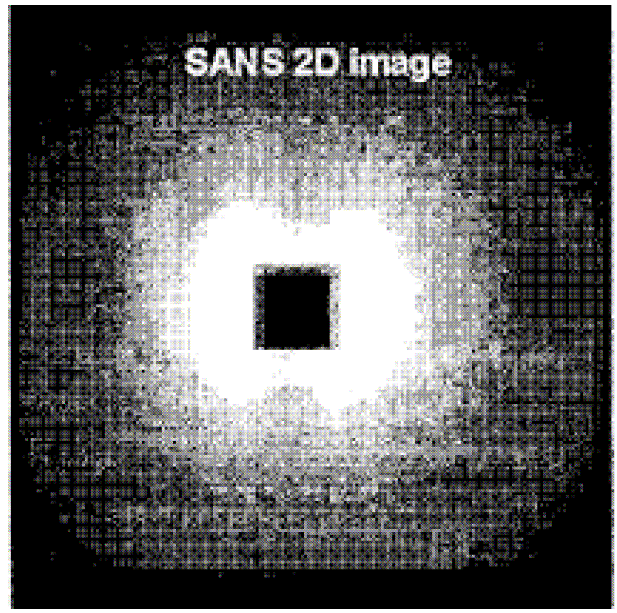

Figure 7: Butterfly scattering pattern measured by Belina et al. Carbon black filled rubber (40%wt) is stretched to a draw ratio of 2.5, reproduced with permission from ref. [72].

The problem of the presence of ZnO in vulcanized elastomers filled with carbon black has been revisited very recently by Morfin et al [74]. In their quite sophisticated approach, they use SANS, SAXS and anomalous SAXS (ASAXS) to disentangle the contributions from ZnO and carbon black. They have performed ASAXS experiments on a synchrotron beamline (D2AM, European Synchrotron Radiation Facility, Grenoble, France). The idea of such experiments is to collect very low angle scattering at different energies of incident irradiation. Seven energies just below the Zn K-edge (9611 eV) were chosen, as well as another one far below (7900 eV). At each energy, SAXS intensities were collected. The latter correspond to different contrast conditions of the ZnO particles, without affecting the contrast of carbon

black. It is thus possible to determine the partial structure factors (essentially CB-CB and ZnO-ZnO, the cross term being negligible). Comparison with ZnO-free samples and SANS enabled the authors to show in a convincing manner that they can extract the carbon black structure in the presence of ZnO.

In a series of articles, F. Ehrburger-Dolle et al address the question of the deformation of the carbon black filler network [75, 76]. In ref. [75], they start with the study of dispersions of carbon black (N330 at 20%v) in ethylene-propylene (EPR) and styrene-butadiene rubber (SBR). For comparison, samples are also studied with the matrix in the melt-state, i.e. before crosslinking with dicumyl peroxide. The SAXS patterns were obtained on a beamline of the ESRF (Grenoble, France), which is equipped with a CCD-camera for two-dimensional detection. In a different set of experiments on samples from the same batch, the mechanical properties were also investigated.

The scattering of the initial, unstretched sample is shown in Figure 8a for the uncrosslinked EPR matrix filled with carbon black. The sample is isotropic, which is why the regrouped data along two perpendicular directions superimposes nicely over the complete q-range. The data analysis is done by fitting power-laws on the straight portions of the intensity in the log-log representation, and a fractal dimension of 1.5 is found by the authors, i.e. a small dimension than the one found in the case of dilute dispersions (1.8, cf. above). This decrease in the fractal dimension is interpreted by the Ehrburger-Dolle et al as the signature of a network of connected, slightly interpenetrating aggregates. After deformation to $\varepsilon = 0.53$, a beautiful butterfly pattern is detected, corresponding to the intensity curves shown in Figure 8b. As in the work of Belina et al [72], it corresponds to two different power laws of the intensity with q. Parallel to the stretching direction, the exponent has again increased to 1.8, whereas it has further decreased, down to 1, in the perpendicular direction. The explanation put forward by the authors seems rather plausible: At rest, aggregates are slightly interpenetrated, and pulling them apart in the parallel direction disentangles them, and they recover the statistical properties they usually adopt in the dilute state. In the perpendicular direction, aggregates are further compacted, thereby increasing the degree of interpenetration, and thus decreasing the apparent fractal dimension. In this context, it might be helpful to point out that the concept of fractals might not be the most appropriate one to describe the specific situation [77]. Technically, the power laws observed in the intensity do not extend over a very large q-range. Intuitively, the decrease of the intensity to a lower power law exponent seems to be more

related to a decrease in density fluctuations due to interpenetration (densification) of aggregates. This is quite opposite to the decrease in density as suggested by the lower fractal dimension. Additional low-q experiments would be necessary to decide on this issue.

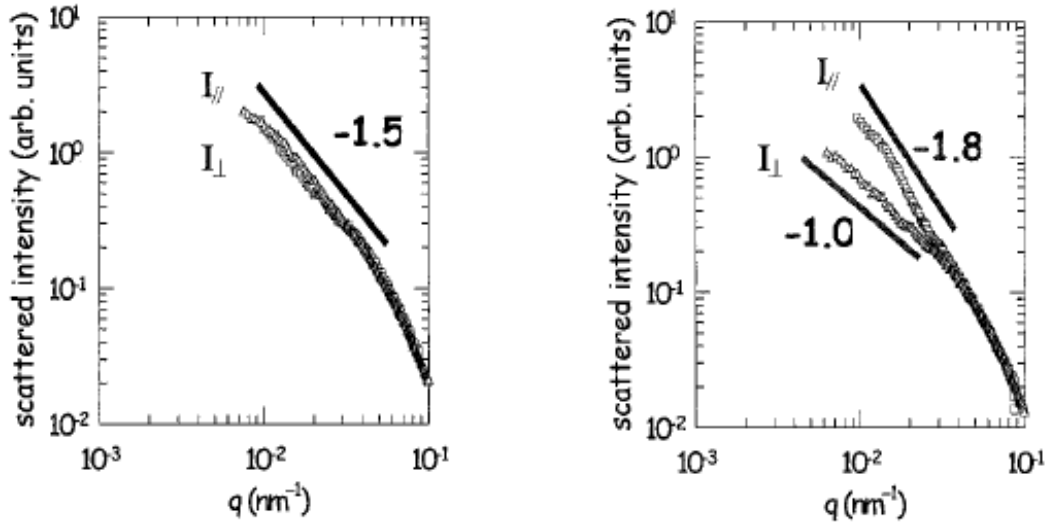

(a) (b)

Figure 8: (a) SAXS intensity curves determined along the two directions (parallel and perpendicular to the direction of stretch) for the initial sample and (b) for the sample stretched to ε = 0.53. Reproduced with permission from ref. [75].

As indicated above, Ehrburger-Dolle et al [75] explore the behavior of the system for different matrices, and also different fillers (carbon black N330, and fumed hydroxylated and hydrophobized silica). As far as the crosslinking of the matrix is concerned, it is found that crosslinked matrices are always isotropic in the deformation range under study (up to ε ≈ 0.5, depending on the sample), for both EPR and SBR, with slightly smaller interpenetration in the case of SBR. In the melts, the isotropic to butterfly evolution is clearly present, and its appearance seems to be correlated with a maximum in the stress-strain curves measured on the same samples.

In a further paper, F. Ehrburger-Dolle et al report on carbon-black composites in HDPE [76], i.e. they use the same matrix as Beaucage [70]. As the latter, samples are prepared by melt blending the carbon black, but they also studied composites produced by solvent casting and composites of carbon black and ethylene-propylene rubber (EPR). The carbon black volume fractions of depelletized N330 of primary particle size 270 Å are between 5 and 30%v. In

their scattering experiments, they use two-dimensional detection, which allows them to focus on anistropy.

On the scale of the carbon black aggregates, the HDPE-composites are isotropic when prepared from solutions; they are anisotropic, with butterfly-like scattering, for samples prepared from melts with high concentrations of carbon black (>15%). This anisotropy is probably introduced through shearing of the melt. When looking at the scattering parallel and perpendicular to the observed anisotropy, power laws with exponent of –1.0 and –1.7 were found, whereas the solvent cast sample had an exponent of –1.2. Faithfully to their interpretation in terms of aggregate interpenetration [75], the authors deduce that there is a spontaneous difference in aggregate interpenetration along these directions. As a second point, the authors have identified the crossover from the mass fractal to the surface scattering of exponent –3.2 using a Kratky presentation of the data, plotting $q^2I(q)$ vs q. Given the absence of a structural model, it is difficult to attach a physical significance to the position of the maximum in this representation. Nonetheless, the plot of this maximum position as a function of carbon black volume fraction evidences two domains, the separation at around 10% coinciding with the percolation threshold as seen by electrical conductivity measurements. Below 10%, no anisotropy is observed, even for stretched samples.

Contrary to these observations, the melt-prepared EPR-nanocomposites at rest hardly show anisotropy even at high filler volume fractions. Upon streching, however, nice butterfly patterns are observed at high concentration (20%), whereas isotropy is conserved at low concentration (5%). This can be understood with rather strong carbon black aggregates, which remain unperturbed if they are spatially isolated. At higher concentrations, they probably interpenetrate, thereby transmitting higher stresses, which leads to shape deformations. In the scattering, the butterfly pattern is due to the strong increase of the corresponding power law at low q (from close to 1 to 1.5), and a much weaker decrease in the perpendicular direction. As before [75], it is interpreted as the signature of disinterpenetration along the stretching direction. The authors use the characteristic wave vector given by the position of the maximum of $q^2I(q)$ in order to deduce a local Poisson ratio, which is found to be about 0.2, close to values obtained with gels. Given that the overall Poisson ratio needs to be close to 0.5 due to volume conservation of elastomers under low stresses, this implies that much of the deformation is supported by the polymer matrix.

To summarize the studies presented in this section, the multi-level structure of carbon blacks in elastomers is rather well described theoretically, namely by Beaucage's expression. Among the difficulties with carbon black data interpretation, one should keep in mind the ongoing discussion about the relationship between primary particle polydispersity and the apparent surface scattering at high-q. The evolution of carbon black structure under strain is much less understood, mainly for two reasons. The first is the complexity encountered with the different matrix-filler couples, which generates qualitatively different scenarios due to the transmission or not of stress down to individual aggregates. The second is related to the difficulties with the analysis of two dimensional data, where both quantitative and convincing models are still missing.

IV.3 Structure of silica

Although carbon black is the traditional filler for elastomer reinforcement, silica becomes more and more popular in industrial applications and fundamental studies. Among the possible reasons one may quote that silica has different surface properties – it is hydrophilic in the bare state – which leads to a different surface chemistry and different polymer–filler interactions. Note that hydrophobized silica can be obtained quite directly by grafting silanes on the surface OH-groups called silanols [19, 78]. Another difference from carbon black is that it can be generated inside the matrix, e.g. from the precursor tetraethoxysilane (TEOS) [62, 79], and the physical-chemical conditions of the silica formation, namely the pH, have a strong influence on the final silica structure. Still another way to control the structure of the silica filler is to control the aggregation of the particles, using sol-gel techniques to incorporate the particles (e.g., solvent casting). In the introduction to this section, we have cited work by Pu et al [59] which demonstrates this possibility. In the coming section, we will discuss scattering studies of the spatial organization of silica beads in polymer matrices, covering the spectrum from completely dispersed model nanoparticles [80] to highly aggregated ones [81]. In the latter case, different modelling approaches can be chosen. As with carbon black, fractal modelling [40-42, 48] may be appropriate in certain cases, whereas dense aggregates with close-packed structures [36, 37] can be described by the methods taken from the theory of simple liquids [30, 31, 36, 37]. Articles on silica-latex nancomposites will also be reviewed [33, 81-85], where controlled aggregation is used to organize silica nanobeads in a polymer matrix. The structural analysis of this system –although being a

model system - is rather complex, and we will develop in this section the basics of Reverse Monte Carlo modelling used to unveil the structure from the scattering.

IV.4 Structure of silica in polymer nanocomposites

We now review investigations of silica-filled polymer matrices where scattering was successfully used to unravel the filler structure. The general principle of small angle scattering and data analysis in filler-polymer nanocomposites have been explained and applied to silica-siloxane composites by Schaefer et al [79]. This group has made significant contributions to mechanical properties of model elastomers, in the filled and unfilled state, where scattering techniques were decisive for the structural analysis of the filler. In the cited reference, the authors discuss both general features of scattering curves (cf. section II), and the scattering signatures of different growth scenarios of a in-situ created filler phase, like nucleation and growth, spinodal decomposition, or kinetic systems. The authors present several classes of what they called silica-siloxane molecular composites, following different synthetic protocols. A prominent example is given by an in-situ filled poly(dimethylsiloxane) (PDMS) network made by end-crosslinking (curing) 18k chains. These networks were then filled by first swelling in pure tetraethylorthosilicate (TEOS), and subsequently placing swollen strips in acid or basic water solutions (pH 2.5 or 11). This process is called in-situ generation of fillers [62]. It leads to an acid- or base-catalyzed precipitated silica filler, the structure of which was measured by small angle scattering. The scattering profiles obtained under acid and basic conditions are quite different, although we will see in the discussion below that the simple picture of pH-sensitivity did not withstand more elaborate investigations [86, 87]. In the acid case, the high-q regime is usually close to a Porod power law q^{-4}, i.e. the formation of a smooth silica-siloxane interface is detected. Under basic conditions, the slope in the high-q regime is close to 4.5, indicating a diffuse silica-polymer interface. This was modelled by Schaefer et al as an interface layer of thickness 10 Å, using a sigmoidal concentration profile. Then the specific surface can be estimated in the two cases, and the resulting Porod radius, i.e. the radius of a monodisperse sphere of same specific surface, compares well with the Guinier radius, both less then 10 nm. The authors have also followed the time development of the same samples with a vapour-catalyzed sample. The striking result is that large-scale structure are visible well before particles, identified by the smooth interfaces leading to Porod scattering, appear. This hints at a very early phase separation of precursor oligomers inside the siloxane network.

The same group has continuously contributed to the field of polymer nanocomposites over the last decades. Here we briefly review two related articles of the mid-nineties [86, 87], where the synthesis, structure and stress-strain isotherms of hybrid organic-inorganic based on polysiloxanes are presented. In the first article [86], elastomers containing silica are investigated, whereas titania fillers are studied in the second one [87]. Various synthesis routes have been followed, e.g. varying the number of stages, i.e. simultaneous curing and filling, or not, using in-situ precipitation. The authors start their first paper with a review of the theory of mass and surface fractal scattering for the analysis of SAXS and SANS data, cf. eqs. (17) and (18). It would exceed the scope of this review if we tried to report all experimental results here. The authors' main conclusion are that (i) polymerization properties of silicates in PDMS are different from solution polymerization, the pH namely being not always the dominant parameter, (ii) it is difficult to achieve not phase-separated systems, which appear to be possible only at low loadings (<5%) and acid catalysis, and (iii) at first glance quite surprisingly, best mechanical properties are obtained with microphase-separated systems, if possible interpenetrated. Similar results are obtained with titania in poly(methylphenylsiloxane) [87], which appears to be less reinforcing than silica with comparable concentration and domain size.

In a more recent article, Schaefer et al discuss the challenges and opportunities in silica-reinforced elastomers [88]. Using SAXS, ultra small angle x-ray scattering (USAXS), and light scattering, these authors follow the evolution of the structure of silica, from powders, to silica in solution, and finally to silica incorporated into styrene butadiene rubber (SBR). The combination of the different scattering techniques allows the structural characterization over up to six orders of magnitude. The silica powders prepared by neutralization of sodium silicate, a precipitate used in the car tire industry, have also been studied by TEM. This technique revealed a complex structure consisting of 100 Å particles aggregated into clusters of 10–100 primary particles. At higher level of structure, the aggregates are lumped into agglomerates that are 'visible' in the scattering data, but hard to see in the real-space micrographs. In the intensity, three length scales can be identified, and using Beaucage's fractal model (eqs. (25) and (26)), these can be related to (i) the smooth primary colloidal particles (R_G = 85 Å), (ii) which are clustered into mass-fractal aggregates of dimension 2.5, (iii) which are further clustered into uniformly dense, but porous objects with surface fractal dimension 2.65 and a radius of gyration of about 20 microns. When dispersed in solution, the

highest level of the silica structure can be broken up by sonification, but the bunch-of-grapes structure of the aggregates remains, indicating strong silica-silica bonds. Upon dispersion of the powder in SBR, finally, the large scale agglomerates are completely disrupted, but the aggregates are found intact. The authors conclude that these aggregates are thus sufficiently robust to survive conventional mixing processes.

A quite different approach is chosen by Persello et al who work with model home-made silica dispersion of particle size 27 nm [37]. The suspensions were mixed with aqueous and basic poly(vinyl alcohol) (PVA) solutions, followed by solvent evaporation, yielding silica volume fractions of up to 25%. Independently, the authors have shown that PVA adsorbs weakly on the particle surface in solution at pH 9. The morphology of the silica filled PVA was then investigated by SANS and TEM. The micrographs at low volume fraction show the formation of silica clusters, the signature of which is a two level Porod scattering in reciprocal space. Although the q-range is somewhat restricted in this experiment, the scattered intensity is found to decrease strongly (q^{-4}) at low q, with a shoulder or very soft maximum at intermediate q, before decreasing again at high q. The authors have modelled this behaviour by scattering from large and dense aggregates, the internal structure of which is the one of a hard sphere fluid described by the Percus-Yevick structure factor. Such models have been developed for silica clusters in solution [36]. The shoulder at intermediate q is related to the nearest neighbour distance inside a cluster. As the bead size is known, the internal volume fraction of the clusters is the only unknown parameter of this function, and it was determined as a function of total volume fraction Φ_{si}. The authors find monotonously increasing values with Φ_{si}, between 40 and 70%. Although the chosen q-range is indeed very limited, thereby excluding a direct observation of the cluster size, the authors have determined the ratio of the Porod radii for the first and the second Porod decrease. The notations are somewhat confusing, but the resulting cluster size appears to be an increasing function with Φ_{si}, between 100 and 600 nm.

The group of Montes et al has worked on reinforced silica systems using approximately 50nm Stöber particles linked to poly(ethyl acrylate) [89]. Due to the grafting of the particles, these authors have observed SANS intensities corresponding to dispersed particles. Their approach is very interesting and complementary, as they have combined dynamical, structural and mechanical investigations [90-93]. This has been done in close collaboration with

theoreticians, thereby contributing to the understanding of the relationship between modifications of the glass transition close to particle surfaces and the reinforcement effect [18].

Although car tires are the most prominent example of an industrial application of reinforcement, one may keep in mind that mechanically much weaker components can also contain solid filler particles. This can be done in order to optimise mechanical properties, but also as additive, e.g., for UV-protection, or as colour agent (pigments). An important field are coating, i.e. thin polymer films deposited as protective and/or decorative layer on substrates, e.g. paints. Originally, water-repelling surfaces, thus made of hydrophobic polymer, were made from solutions in volatile organic solvents. The increasing demand for non-toxic solvents lead to the industrial development of aqueous suspensions of sub-micron hydrophobic polymer beads called latex. The colloidal stability of such suspensions is achieved either sterically with hydrosoluble polymer chains grafted on the bead surface [94], or electrostatically with polyelectrolyte groups on the surface. In both cases, the beads have thus a core-shell structure. Such suspensions can be dried slowly, until crack- and bubble-free homogeneous polymer films, possibly millimetre thick polymer films are obtained. This process is called film formation, and takes place above a characteristic temperature called minimum film formation temperature. Pioneering work on latex films is due to researchers at BASF and what is now Rhodia [95-97], and comprehensives reviews are available, e.g. [98]. The mechanical properties of latex films depend on many parameters (T, ion concentrations, maturity …), but they stay in general rather weak. Important reinforcement can be obtained by incorporating hard filler particles, and contrary to filled rubber, the particles can be easily included by a sol-gel route. In this case, the particles are suspended in water, mixed to the latex suspension, and dried. This allows a thermodynamic control of the final film properties, via the particle interaction potential in solution, and does not depend on any energy input through shearing and mixing.

We start the discussion with scattering studies of pure latex films by SANS [99]. Motivated by the water permeation properties of coating, these authors studied the water uptake in the hydrophilic shells. The latter connect during film formation to form a continuous membrane, and depending on the degree of neutralization before film formation, more or less water can be incorporated. The water-uptake is then used to study the structure of the latex films, at rest and under deformation, using SANS. Indeed, by using deuterated water (D_2O), the membrane

gains contrast and the cores become visible in the continuous membrane. As the water-uptake influences the mechanical properties of the polymer, deuterated organic solvents were used for comparison. Due to the well-defined size of the latex particles, which is in turn related to its big size, 1200 Å, the samples are well-ordered cellular films, with quasi-crystallographic diffraction peaks. Upon deformation, rather complicated 2D-diffraction patterns are observed, the structure of which depends on which part (core or membrane) is 'hard' and which is 'soft', i.e. swollen by the solvent. To summarize briefly, latex films have a complicated core-shell structure, where the cores can play the role of a hard filler phase below their T_g and if they are not swollen by solvent ('self-reinforcement'). If hard mineral particles are incorporated, however, then the latex film can be looked at as a soft, homogeneous polymer matrix.

In a second publication, Rharbi et al study the modes of deformation in a soft/hard nanocomposite [100]. The samples are obtained by the process outlined in the preceding paragraph, i.e. by mixing of colloidal stock solutions of latex and silica, and drying. The silica particles of diameter 250 Å were incorporated under acid and basic conditions. As the protonation of the silanol groups on the surface of the silica particles depends on the solution pH, this influences the degree of electrostatic repulsion between the silica particles. These authors have shown by SANS that this is directly related to the degree of aggregation of the silica particles in the latex film. At low pH, the silica is highly aggregated, which gives rise to a strong intensity at low q, whereas the silica is rather well dispersed under basic conditions. The authors also show that the mechanical properties, characterized by stress-strain isotherms, are strongly modified by the silica, and in particular the low pH samples are the most reinforced ones. The modes of deformation of the well-dispersed, high pH sample, at high volume fraction (18%) are then studied using a 2D detection of the small angle intensity. At low deformation ($\lambda = 1.24$) a double-wing intensity is found, and at higher deformation ($\lambda = 2.75$), a striking four-lobe patterns which we reproduce in Figure 9. These have been shown by the authors to be compatible with local rearrangements ('buckling' or 'local shear') of compressed bands of beads, which have been formed by the lateral compression which accompanies the stretching in the parallel direction. These ideas have been checked by numerical simulations [100], and are also discussed in a dedicated article [33].

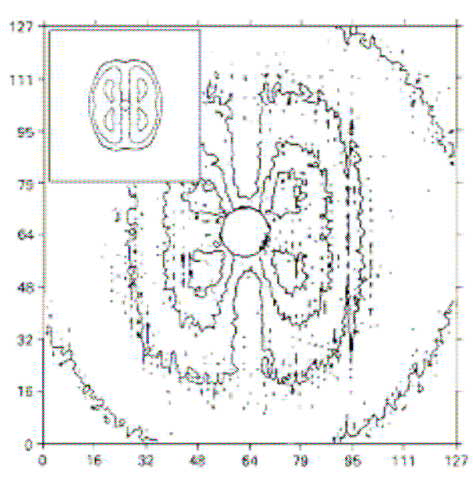

Figure 9: Four-spot intensity contours on a two-dimensional SANS detector for 18%v of silica in latex, stretched to a draw ratio of 2.75, reproduced with permission from ref. [100].

Note that a very similar model system was investigated by Grillet et al who also studied silica-latex films, the morphology of which was checked by optical and scanning electron microscopy [101]. These authors underline the problems arising with the loss of colloidal stability and phase separation during the drying process, and explore different routes of stabilization, namely the use of surfactants and poly(ethylene oxide) as polymeric dispersant, ensuring an additional steric stabilization of particles.

Sophisticated small angle and ultra small angle experiments on silica filled rubber under elongation have been performed at Spring-8 (Hyogo, Japan). Shinorhara et al report on two-dimensional silica-silica structure factors in a q-range starting at 10^{-4} $Å^{-1}$ [102]. In a recent SAXS study of nanocomposites filled with in-situ prepared silica (diameter ca. 34 nm), Ikeda et al show a series of two-dimensional scattering patterns which evolve from butterfly wings into a four spot pattern during elongation [103], just as found by Rharbi et al [100]. In line with the literature, the authors discuss the scattering signatures in terms of sheet formation and buckling, which appears to be the most plausible scenario but suffers of course from the problem that scattering data can not be converted unambiguously in direct-space information. As outlined in section II.2, the analysis of small angle scattering data is always limited due to the fundamental impossibility to find a *unique* structure in agreement with the scattered intensity. In this context, the paper by Le Diagon et al on modes of deformation of silica particles on the surface of an elastomeric matrix is of particular interest [104]. These authors use AFM on stretched nanocomposites and follow the motion of the particles on the surface.

The drawback of the method is of course that motion is limited to two-dimensions, and any bead disappearing or reappearing on the surface may induce artefacts. The calculation of pair correlation functions and the comparison of their Fourier transform to structure factors measured by scattering in other systems is an important and encouraging step to the understanding of real-space motion associated with, e.g., the four-lobe patterns (cf. Figure 9).

Another rather complete study of a silica-latex nanocomposites is also available [44, 81-85]. The system was made of nanolatex (radius about 14nm) and nanosilica beads (about 8 nm). The mechanical properties were characterized by stress-strain isotherms [82, 83], for two silica sizes, silica volume fractions between 2.5 and 15%, and various precursor pH values. The reinforcement factor of Young's modulus, E/E_{latex}, quantifies how much stronger the nanocomposite is with respect to its own, pure matrix. At fixed silica volume fraction, it was shown to vary strongly, e.g. for $\Phi_{si} = 5\%$ from about one at high pH to more than 20 at low pH. A summary of these results has been published in ref. [81]. This strong effect suggests that considerable structural changes at constant fraction of hard matter can be induced in this system, as already recognized by previous authors [100].

The structure of these silica-latex nanocomposites was investigated by SANS [81, 84]. The intensity displays considerable differences with Φ_{si} and pH, which reflects of course the very different structures, i.e. aggregates with different aggregation numbers. The generic shape of the intensity curve is a prominent peak in the low-q range, followed by an intermediate powerlaw-like behaviour up to a cross-over at high q to surface scattering (q^{-4}). The high-q part is of course due to the known particle scattering, whereas the intermediate scattering characterizes the internal structure of aggregates. The strong peak, finally, indicates that there is a well-defined size in the system; in our case it is the most-probable distance between centres of mass of aggregates. As the silica volume fraction is known, the position of the maximum q_o can be used to estimate the average aggregation number: $N_{agg} = (2\pi/q_o)^3 \Phi_{si}/V_{si}$, where V_{si} is the average volume of one silica bead. In a first time, this analysis was carried out for all data, and an almost one-to-one correspondence between precursor pH and N_{agg} could be established. This in turn confirmed the picture outlined above: reinforcement depends strongly on the structure of the filler particles inside the matrix, and the higher the aggregation number, the higher the reinforcement factor E/E_{latex}.

Besides the yet unsolved mystery of the spontaneous formation of well-defined aggregates, two important questions remain concerning these results in the silica-latex system. First, is the rather basic data analysis in terms of the peak position q_o only sufficient ? Is the complete scattering curve compatible with this aggregate picture ? And second, why is there such a strong reinforcement for big aggregates, an idea quite opposed to all modern funding schemes, where the word 'nano' is supposed to be the key to success (and money) ?

To answer these questions, reverse Monte Carlo (RMC) simulations have been performed. RMC (or related approaches) is a method developed for the interpretation of scattering data in the past 15 years [63, 105, 106]. Its principle is illustrated in Figure 10, and more details can be found in a recent reference [44]. The idea is to produce a representation of an aggregate (Figure 10a), to calculate its scattering (Figure 10b), and then to update in a random manner the aggregate structure, by moving a bead to another position. If the agreement between the experimental I(q) and the prediction is improved, then the new position is accepted, otherwise it is discarded. The final fit shown on the right-hand side of Figure 10 illustrates the good quality of the complete fit obtained by this method.

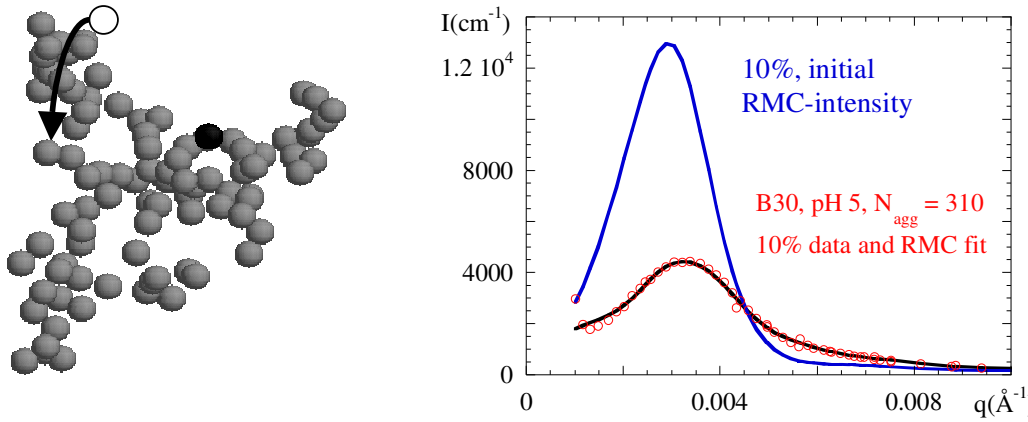

Figure 10: (a) Elementary step of the Reverse Monte Carlo simulation consisting in replacing beads in a random manner. The black bead can not be removed without destroying the aggregate. Apparently isolated beads are drawing artefacts induced by the representation, which does not take bead size polydispersity into account. (b) Effect on scattered intensity, the initial RMC-guess is seen to be very different from the experimental intensity, whereas the final agreement is satisfactory.

Using RMC, we have answered the first of the two questions. The aggregation picture and number are indeed compatible with the complete scattering profile. The impact of aggregation on the mechanical properties (cf. second question) can now also be understood, at least

qualitatively. In Figure 11, a representative real-space picture of aggregates as found by RMC is compared to hypothetical dense spheres containing the same amount of silica.

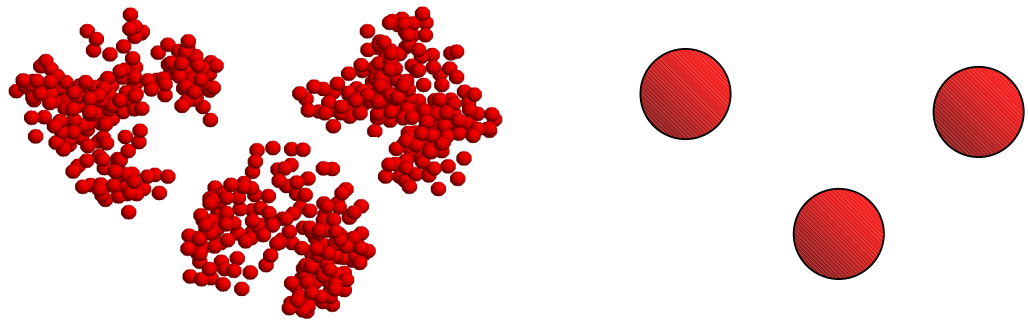

Figure 11: (a) Real space picture of aggregates as a result of the RMC-algorithm, arranged for illustration at distances comparable to the inter-aggregate distance deduced from the scattering peak. (b) The same silica mass per aggregate concentrated in a hypothetical dense sphere, at the same positions. This illustrates the space-filling properties of aggregates, a presumably fundamental issue for the understanding of the mechanical properties of such nanocomposites.

It is clear from the picture that percolating paths of hard matter may be formed under deformation in the aggregated case, which is presumably responsible of the improvement of the mechanical properties. Coming back to the above comment about funding, it seems better to have smaller ("nano") but organized particles, in order to achieve the space-filling properties necessary for higher mechanical reinforcement.

Up to now, we have focussed this review on the structure of the silica particles in the matrix, as there is a strong relationship between the structure and the mechanical properties, e.g. in percolated systems. There is another important contribution to the reinforcement effect, related to the bonding of the polymer matrix to the filler particles. The grafting of polymer chains onto the surface of silica particles is therefore a method to influence bonding properties and filler-matrix compatibility. If one wishes to increase the grafting density, it is favourable to grow the chains simultaneously 'from' the surface by first grafting the initiator, and a recent review has been published on this grafting technique [107]. Scattering can be useful for various reasons. In a recent article, Inoubli et al study the mechanical properties of poly(butylacrylate) filled with grafted silica particles of radius 50 and 12 nm [80]. The grafted chains are of the same nature and mass as the matrix (30k for the smaller silica), and the

authors report that it is not possible, except at very low volume fractions, to incorporate bare silica in the matrix, whereas the grafted silica can be mixed with free polymer in solution, followed by drying. In the scattering experiment only the silica is seen in a polymer background, grafted or not. The SANS data of the filled polymer are consistent with the form factor of single particles, together with a repulsive interaction term, which indicates that particles are well dispersed even at relatively high volume fractions (18%). These results which are confirmed by TEM micrographs. The next step, which is also proposed by the authors, would be to deuterate the grafted chains, in order to 'see' the corona within the matrix using SANS and contrast variation.

Such a study is also the aim of a group working on a slightly different system. El Harrak et al grafted poly(styrene) and poly(butyl methacrylate) on colloidal silica using a controlled radical polymerization [19, 20, 108, 109]. The grafting procedure of styrene using 'grafting from' is described in detail in ref. [20], whereas poly(butyl methacrylate) is studied in ref. [19]. The grafting is followed by contrast matching either the silica core or the polymer, using mixtures of hydrogenated and deuterated solvent. In the case where the silica structure is probed, the dispersion of the particles in the solvent could be checked, whereas in the other case the growth of the polymer layer could be followed, cf. Figure 12. The quantitative analysis of the scattering data, using spherical core-shell models, showed that the silica is slightly aggregated in solution, and that the number density of polymer on the surface is compatible with the grafting density. The growing chain mass could be directly followed in the case where the silica core was matched, and was found to grow in accordance with the results of the chemical analysis, using chain etching and chromatography. Moreover, a purification process was shown to be efficient to produce single grafted particles, as evidenced by SANS. As with the work by Inoubli [80], the next step should be the incorporation of labelled chains in an unlabelled matrix, in order to investigate the behaviour of the grafted layer inside the – possibly deformed – nanocomposite.

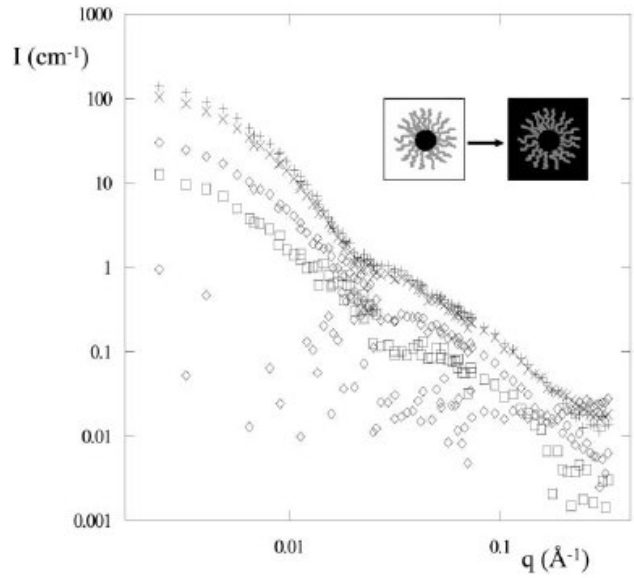

Figure 12: Check of polymer growth: scattered intensity in silica matching conditions for successive polymerization times. The increase in the signal goes with the growth of the polymer layer on the invisible (due to matching) silica particles. Reprinted from ref. [19] – Reproduced by permission of The Royal Society of Chemistry.

The studies of silica structure in nanocomposites by small-angle scattering has been reviewed in this section. In comparison to carbon black, silica is found to be more appropriate for model systems, namely because the synthesis allows for a tighter control of the primary bead size and surface properties, and particle aggregation. Recent progress in the field of colloidal chemistry, with controlled grafting of polymer *from* the particles surface has been reviewed, and this is expected to lead to nanocomposites with new, hopefully improved properties. More complex structures of silica inside nanocomposites have also been described recently, using either standard theory of liquids, fractal models, or Reverse Monte Carlo. It is hoped that this will trigger research on the structure of deformed silica nanocomposites, where many features are described only qualitatively at the moment. In fine, this might lead to a detailed understanding of the relationship between the evolution of filler structure under strain and the reinforcement effect.

IV.5 Structure of clay and polymeric fillers in polymer nanocomposites

In this last section of the chapter we review both clay and polymeric filler as seen by small-angle scattering. Neither one of these subjects is currently sufficiently developed to justify a

section of its own. Clay or layered silicates are nanometer-thin platelets of large lateral dimension, typically of the order of hundreds of nanometers. The incorporation of clay particles in polymer matrices has promising applications, which is probably why the advent of polymer-clay hybrids has triggered large research efforts over the past years [110]. However, the method usually preferred for structural analysis appears to be electron microscopy, e.g. TEM on thin slices, sometimes combined to wide angle scattering. The idea behind wide-angle scattering is that the clay layers are usually arranged in stacks (or tactoids), with a typical repeat distance of a few nanometers, which leads to a peak in the scattered intensity. In spite of a large body of experimental evidence with clay-polymer hybrids, the data analysis goes rarely beyond the following triplet: (i) If the location of the scattering peak corresponds to the distance measured in dry clay, then the stacks have been dispersed as a whole in the polymer matrix. (ii) If the peak persists but shifts to smaller angles, than some polymer (or additives) has been intercalated between the platelets. And finally, (iii), if the peak disappears, then the clay is said to be completely exfoliated. Note, however, that some studies concentrating on large-scale structures exist [111, 112].

In the past, several teams have attempted to give a more quantitative description of the scattered intensity in polymer-clay hybrids [111, 113, 114], or in solvents, where the same concepts apply [35, 115]. We start the discussion with the papers by Ho et al and Hanley et al [35, 115], where the scattering of clay particles as individual cylinders or in stacks is described. The fundamental equation for the structure factor arising from the correlations between neighboring platelets inside a tactoid can be calculated as following Kratky and Porod [116]:

$$S(q) = 1 + \frac{2}{N}\sum_{k=1}^{N}(N-k)\cos(kDq\cos\varphi)\exp\left(-k(q\cos\varphi)^2\sigma_D^2/2\right) \qquad (27)$$

where ϕ is the angle between q and the axis of the tactoid, N corresponds to the total number of platelets stacked, and D and σ_D represent the next neighbor center-to-center distance and its Gaussian standard deviation, respectively. The total coherent scattered intensity can then be calculated by straightforward integration for randomly oriented individual tactoids in dilute dispersion. The generic scattering profiles found by these authors are characterized by the absence of a low-q plateau because structures are too big to be seen in this q-range, a q^{-2} decrease at low-q characteristic of the platelet form factor, and a high-q peak (around 1.3 nm^{-1}) caused by the correlations inside each tactoid (repeat distance 5 nm) [35, 115]. The exact height of the peak depends on the average number of platelets inside each tactoid, which

allows the authors to conclude that there are typically about three to six Montmorillonite platelets in one tactoid [115].

Among the articles proposing a quantitative analysis of small-angle scattering from clay dispersion in water or (potentially) in nanocomposites [113, 114, 117, 118], we now discuss the work by Hermes et al [111] because it focuses on the low-q part. These authors present a quantitative model for fitting small-angle data of montmorillonite platelets dispersed as individual platelets and or tactoids. Due to the large lateral dimensions of the platelets, a few hundred nanometers, a Guinier-type low-q scattering is out of reach with standard small-angle set-ups; moreover, it would be visible only at low concentrations of individually dispersed platelets. Contrary to other studies, the authors were interested and successfully described the low-q scattering, which is of course directly related to the dispersion of the platelets in the matrix, as opposed to high-q scattering probing nearest neighbour correlations.

The model by Hermes et al [111] focuses on the appearance of tactoids as whole particles, ignoring correlations between tactoids at still larger length scales. For simplicity, the internal structure of tactoids is assumed to be regular, as deviations from regularity would only effect the high-q scattering. We refer to the original article for a detailed description of the (analytical) formulas involved in the modelling. The authors use this formalism to investigate the effect of the presence of tactoids, with increasing portions of platelets per tactoid. Among the results one may cite the deviations from strict q^{-2} scattering at low q induced by the presence of tactoids. After a thorough discussion of the scattering length densities and possible H/D exchange, the formalism is then applied to aqueous dispersions of Montmorillonite. A typical result is shown in Figure 13, where a good fit of small-angle data is obtained with a dispersion of individual platelets and small tactoids.

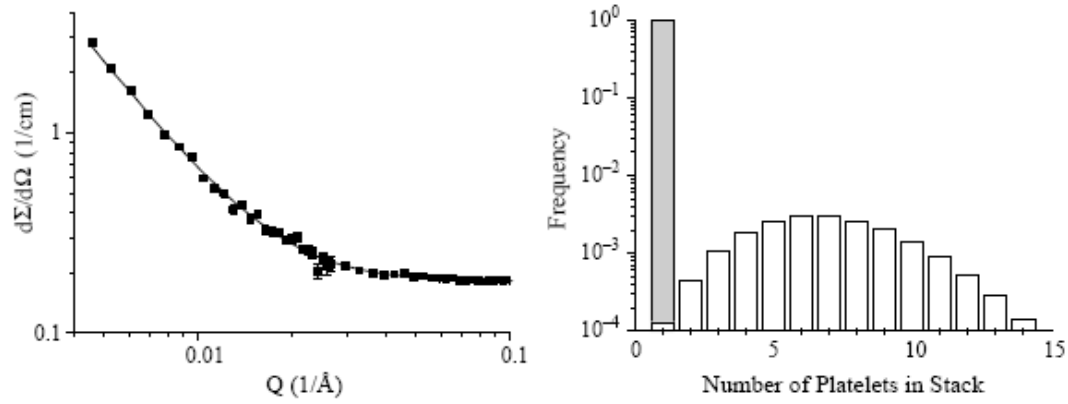

Figure 13: (a) typical fit (line) to data (symbols) from Montmorillonite in 85% D_2O dispersion (b) illustration of platelet distribution used in fit. Reprinted from ref. [111] with permission from Elsevier.

To finish the section, we now turn to a few studies of the structure of polymeric fillers [101, 119-121]. Note that a large body of literature on self-organizing block copolymer structures exists, leading to spherical, cylindrical or locally lamellar morphologies [122-125]. Such systems have been studied also under deformation using mainly SAXS. If one of the blocks is a high-Tg polymer (e.g. PS or PMMA), and the other one an elastomer at room temperature (e.g., poly(butadiene)), then self-reinforcing systems of possibly highly complex morphologies may be obtained [126]. Such self-organized systems are outside the scope of this review and we focus on chemically simpler systems. Chevalier et al have studied mixed latex films similar to the silica-latex films discussed above, where one component was butyl acrylate latex, the other polystyrene latex [101, 119]. The glass transition temperatures (T_g) of the two components being quite different, the system is a soft matrix with hard spherical inclusions at any intermediate temperature. Using different protocols, as well as a core-shell latex of similar composition, and annealing some of the samples above the T_g of the PS, the authors could show by SANS that different structures of the hard PS domains could be created inside the film. The annealed samples, e.g., have finite-size PS domains (no low-q upturn), but have lost all nearest neighbor correlations between beads, indicating that the PS beads have been molten and merged into groups. On the other hand, aggregated samples display the bead-bead interaction peak, which could be modeled by clusters of beads with hard-sphere repulsion and with a high internal volume fraction of 60% (cf. ref [36]).

Another scattering study with polymeric filler has been published by Blundell et al [127]. This group has investigated thermoplastic polyurethanes at rest and at large strains. They compare

two samples, one made of randomly copolymerized monomers, the other with a block copolymer architecture, the different parts having different glass transition temperatures leading to a soft/hard nanocomposite. The observed mesophases are due to yet not perfectly understood ripening processes within the samples, on scales of typically 10 nm, i.e. well adapted to SAXS. The mechanical response is surprisingly similar in both cases. The evolution of the microstructure, however, is quite spectacular, with observations very similar to the ones described by others [33, 100]. Affine displacement and deformation of domains leading to ellipsoidal scattering patterns, and in the case of the sample with alternating blocks, an intriguing four-spot pattern. The behavior with strain of the latter is investigated in detail by the authors, but no simple explanation its interpretation was given.

V. Concluding remarks

Recent advances in the analysis of filler particle morphologies (carbon black, silica, polymeric fillers and clay) and network structure in polymer nanocomposites with Small Angle Scattering have been reviewed. It appears that scattering is a powerful tool, which is used with success in systems of ever increasing complexity in terms of dispersion, particle shape and polydispersity, and number of components. It is clear that a certain degree of both experimental and theoretical technicality is required in order to extract information from the scattering curves. We think, however, to have given a sufficiently broad introduction on how useful scattering can be, which technique is to be chosen, and how the data modeling can be handled. To summarize, we hope to have indicated some promising directions and opened some useful paths in the mountainous (reciprocal space-) landscape of prominent peaks, perfidious plateaus, and slippery slopes.

VI. References

1. Mark, J.E., B. Erman, and F.R. Eirich, *Science and Technology of Rubber*, ed. J.E. Mark. 1994, San Diego: Academic Press.
2. Guth, E., *Theory of Filler Reinforcement.* Journal of Applied Physics, 1945. **16**: p. 20-25.
3. Heinrich, G., M. Kluppel, and T.A. Vilgis, *Reinforcement of elastomers.* Current Opinion in Solid State & Materials Science, 2002. **6**(3): p. 195-203.
4. Boonstra, B.B., Polymer, 1979. **20**: p. 691.
5. Voet, A., *Reinforcement of Elastomers by Fillers - Review of Period 1967-1976.* Macromolecular Reviews Part D-Journal of Polymer Science, 1980. **15**: p. 327-373.
6. Schmidt, G. and M.M. Malwitz, *Properties of polymer-nanoparticle composites.* Current Opinion in Colloid & Interface Science, 2003. **8**(1): p. 103-108.
7. Kohls, D.J. and G. Beaucage, *Rational design of reinforced rubber.* Current Opinion in Solid State & Materials Science, 2002. **6**(3): p. 183-194.
8. Witten, T.A., M. Rubinstein, and R.H. Colby, *Reinforcement of Rubber by Fractal Aggregates.* Journal De Physique Ii, 1993. **3**(3): p. 367-383.
9. Blanchard, A., R.S. Graham, M. Heinrich, W. Pyckhout-Hintzen, D. Richter, A.E. Likhtman, T.C.B. McLeish, D.J. Read, E. Straube, and J. Kohlbrecher, *Small angle neutron scattering observation of chain retraction after a large step deformation.* Physical Review Letters, 2005. **95**(16): p. -.
10. Boue, F., J. Bastide, M. Buzier, C. Collette, A. Lapp, and J. Herz, Progress in Colloid and Polymer Science, 1987. **75**: p. 152.
11. Doi, M. and S.F. Edwards, *The Theory of Polymer Dynamics*. 1986, Oxford: Oxford University Press.
12. Ahmed, S. and F.R. Jones, *A Review of Particulate Reinforcement Theories for Polymer Composites.* Journal of Materials Science, 1990. **25**(12): p. 4933-4942.
13. Smallwood, H.M., J Appl Phys, 1944. **15**: p. 758-766.
14. Einstein, A., Ann. Phys., 1906. **19**: p. 289.
15. Medalia, A.I., Rub Chem Tech, 1974. **47**: p. 411.
16. Polmanteer, K.E. and C.W. Lentz, Rub Chem Techn, 1975. **48**: p. 795.
17. Berriot, J., H. Montes, F. Lequeux, D. Long, and P. Sotta, *Evidence for the shift of the glass transition near the particles in silica-filled elastomers.* Macromolecules, 2002. **35**(26): p. 9756-9762.
18. Long, D. and F. Lequeux, *Heterogeneous dynamics at the glass transition in van der Waals liquids, in the bulk and in thin films.* European Physical Journal E, 2001. **4**(3): p. 371-387.
19. Carrot, G., A. El Harrak, J. Oberdisse, J. Jestin, and F. Boue, *Polymer grafting from 10-nm individual particles: proving control by neutron scattering.* Soft Matter, 2006. **2**(12): p. 1043-1047.
20. El Harrak, A., G. Carrot, J. Oberdisse, C. Eychenne-Baron, and F. Boue, *Surface-atom transfer radical polymerization from silica nanoparticles with controlled colloidal stability.* Macromolecules, 2004. **37**(17): p. 6376-6384.
21. Oberdisse, J., *Adsorption and grafting on colloidal interfaces studied by scattering techniques.* doi:10.1016/j.cocis.2006.11.001, 2007.
22. Guinier, A. and G. Fournet, *Small-Angle Scattering of X-Rays*. 1955: John Wiley & Sons.
23. Lindner, P., *Neutrons, X-ray and Light Scattering*, ed. P. Lindner and T. Zemb. 2002: North Holland, Elsevier.

24. Benoit, H.C. and J.S. Higgins, *Polymers and neutron scattering.* 1994, Oxford: Oxford University Press.
25. Glatter, O. and O. Kratky, *Small Angle X-Ray Scattering*. 1982, London: Academic Press.
26. Hansen, J.P. and I.R. McDonald, *Theory of Simple Liquids*. 1986, London: Academic Press.
27. d'Aguanno, B. and R. Klein, J. Chem. Soc. Faraday Trans., 1991. **87**: p. 379.
28. Debye, P., Phys. Coll. Chem., 1947. **51**: p. 18.
29. Percus, J.K. and G.J. Yevick, *Analysis of Classical Statistical Mechanics by Means of Collective Coordinates.* Physical Review, 1958. **110**(1): p. 1-13.
30. Hansen, J.P. and J.B. Hayter, *A Rescaled Msa Structure Factor for Dilute Charged Colloidal Dispersions.* Molecular Physics, 1982. **46**(3): p. 651-656.
31. Hayter, J.B. and J. Penfold, *An Analytic Structure Factor for Macroion Solutions.* Molecular Physics, 1981. **42**(1): p. 109-118.
32. Klüppel, M., *The Role of disorder in Filler Reinforcement of Elastomers on Various Length Scales.* Adv Polym Sci, 2003. **164**: p. 1-86.
33. Oberdisse, J., Y. Rharbi, and F. Boue, *Simulation of aggregate structure and SANS-spectra in filled elastomers.* Computational and Theoretical Polymer Science, 2000. **10**(1-2): p. 207-217.
34. Berret, J.F., P. Herve, O. Aguerre-Chariol, and J. Oberdisse, *Colloidal complexes obtained from charged block copolymers and surfactants: A comparison between small-angle neutron scattering, Cryo-TEM, and simulations.* Journal of Physical Chemistry B, 2003. **107**(32): p. 8111-8118.
35. Ho, D.L., R.M. Briber, and C.J. Glinka, *Characterization of organically modified clays using scattering and microscopy techniques.* Chemistry of Materials, 2001. **13**(5): p. 1923-1931.
36. Wong, K., P. Lixon, F. Lafuma, P. Lindner, O.A. Charriol, and B. Cabane, *Intermediate Structures in Equilibrium Flocculation.* Journal of Colloid and Interface Science, 1992. **153**(1): p. 55-72.
37. Persello, J., J.P. Boisvert, A. Guyard, and B. Cabane, *Structure of nanometric silica clusters in polymeric composite materials.* Journal of Physical Chemistry B, 2004. **108**(28): p. 9678-9684.
38. Jullien, R. and R. Botet, *Aggregation and Fractal Aggregates*. 1987: Singapore: World Scientific.
39. Schmidt, P.W., *Small-Angle Scattering Studies of Disordered, Porous and Fractal Systems.* Journal of Applied Crystallography, 1991. **24**: p. 414-435.
40. Teixeira, J., *Small-Angle Scattering by Fractal Systems.* Journal of Applied Crystallography, 1988. **21**: p. 781-785.
41. Beaucage, G., *Approximations Leading to a Unified Exponential/Power-Law Approach to Small-Angle Scattering.* J. Appl. Cryst., 1995. **28**: p. 717-728.
42. Dimon, P., S.K. Sinha, D.A. Weitz, C.R. Safinya, G.S. Smith, W.A. Varady, and H.M. Lindsay, *Structure of Aggregated Gold Colloids.* Physical Review Letters, 1986. **57**(5): p. 595-598.
43. de Gennes, P.G., *Scaling Concepts in Polymer Physics*. 1979, Ithaca, New York: Cornell University Press.
44. Oberdisse, J., P. Hine, and W. Pyckhout-Hintzen, *Structure of interacting aggregates of silica particles for elastomer reinforcement.* Soft Matter, 2007. **2**: p. 476-485.
45. Botti, A., W. Pyckhout-Hintzen, D. Richter, V. Urban, E. Straube, and J. Kohlbrecher, *Silica filled elastomers: polymer chain and filler characterization in the undeformed state by a SANS-SAXS approach.* Polymer, 2003. **44**(24): p. 7505-7512.

46. Botti, A., W. Pyckhout-Hintzen, D. Richter, V. Urban, and E. Straube, *A microscopic look at the reinforcement of silica-filled rubbers.* Journal of Chemical Physics, 2006. **124**(17): p. 174908.
47. Warner, M. and S.F. Edwards, J. Phys. A: Math. Gen., 1978. **11**: p. 1649.
48. Beaucage, G., *Small-angle scattering from polymeric mass fractals of arbitrary mass-fractal dimension.* Journal of Applied Crystallography, 1996. **29**: p. 134-146.
49. Quan, X. and J. Koberstein, J. Polym. Sci. Part B: Pol. Physics, 1987. **25**: p. 1381-1394.
50. Quan, X., I. Gancarz, J. Koberstein, and G. Wignall, J. Polym. Sci. Part B: Pol. Physics, 1987. **25**: p. 641-650.
51. Williams, C., M. Nierlich, J.P. Cotton, G. Jannink, F. Boue, M. Daoud, B. Farnoux, C. Picot, P.G. De Gennes, M. Rinaudo, M. Moan, and C. Flow, J. Polym. Sci. Lett., 1979. **17**: p. 379.
52. Ackasu, A., G. Summerfield, S. Jahsan, C. Han, C. Kim, and H. Yu, J.Polym. Sci. Polym. Physic. ed., 1980. **18**: p. 863.
53. Quan, X., J. Miller, and S. Cooper, Polymer, 1985. **26**: p. 1915.
54. Nakatani, A., W. Chen, R. Schmidt, G. Gordeon, and C. Han, Internat. J. of Thermophysics, 2002. **23**: p. 199.
55. Nakatani, A., W. Chen, R. Schmidt, G. Gordon, and C. Han, Polymer, 2001. **42**: p. 3713-3722.
56. Westermann, S., M. Kreitschmann, W. Pyckhout-Hintzen, D. Richter, E. Straube, B. Farago, and G. Goerigk, *Matrix chain deformation in reinforced networks: a SANS approach.* Macromolecules, 1999. **32**(18): p. 5793-5802.
57. Sen, S., Y. Xie, S.K. Kumar, H. Yang, A. Bansal, D.L. Ho, L. Hall, J.B. Hooper, and K.S. Schweizer, *Chain Conformations and Bound-Layer Correlations in Polymer Nanocomposites.* Phys Rev Lett, 2007. **98**: p. 128302.
58. Hjelm, R.P., P.A. Seeger, and W.A. Wampler, *Microstructure of Composite Materials Using Small-Angle Neutron Scattering and Contrast Variation: Approaches Toward Understanding the Structure of Carbon Black-Elastomer Mixtures.* Polymers and Polymer Composites, 1993. **1**(1): p. 53A-69A.
59. Pu, Z.C., J.E. Mark, J.M. Jethmalani, and W.T. Ford, *Effects of dispersion and aggregation of silica in the reinforcement of poly(methyl acrylate) elastomers.* Chemistry of Materials, 1997. **9**(11): p. 2442-2447.
60. Huber, G. and T.A. Vilgis, *On the mechanism of hydrodynamic reinforcement in elastic composites.* Macromolecules, 2002. **35**(24): p. 9204-9210.
61. Huber, G., T.A. Vilgis, and G. Heinrich, *Universal properties in the dynamical deformation of filled rubbers.* Journal of Physics-Condensed Matter, 1996. **8**(29): p. L409-L412.
62. Mark, J.E., C.Y. Jiang, and M.Y. Tang, *Simultaneous Curing and Filling of Elastomers.* Macromolecules, 1984. **17**(12): p. 2613-2616.
63. McGreevy, R.L., *Reverse Monte Carlo modelling.* Journal of Physics: Condensed Matter, 2001. **13**: p. R877-R913.
64. Medalia, A.I., *Effective volume of aggregates of carbon black from electron microscopy; application to vehicle adsorption and to die swell of filled rubber.* Journal of Colloid and Interface Science, 1970. **32**: p. 115-131.
65. Rieker, T.P., S. Misono, and F. Ehrburger-Dolle, *Small-angle X-ray scattering from carbon blacks: Crossover between the fractal and Porod regimes.* Langmuir, 1999. **15**(4): p. 914-917.

66. Hoinkis, E., E.B.F. Lima, and P. Schubert-Bischoff, *A study of carbon black corax N330 with small-angle scattering of neutrons and X-rays.* Langmuir, 2004. **20**(20): p. 8823-8830.
67. Donnet, J.B., M.J. Wang, E. Papirer, and A. Vidal, *Influence of Surface-Treatment on the Reinforcement of Elastomers.* Kautschuk Gummi Kunststoffe, 1986. **39**(6): p. 510-515.
68. Luo, H., M. Kluppel, and H. Schneider, *Study of filled SBR elastomers using NMR and mechanical measurements.* Macromolecules, 2004. **37**(21): p. 8000-8009.
69. Schaefer, D.W., T. Rieker, M. Agamalian, J.S. Lin, D. Fischer, S. Sukumaran, C.Y. Chen, G. Beaucage, C. Herd, and J. Ivie, *Multilevel structure of reinforcing silica and carbon.* Journal of Applied Crystallography, 2000. **33**(1): p. 587-591.
70. Beaucage, G., S. Rane, D.W. Schaefer, G. Long, and D. Fischer, *Morphology of polyethylene-carbon black composites.* Journal of Polymer Science Part B-Polymer Physics, 1999. **37**(11): p. 1105-1119.
71. Hindermann-Bischoff, M. and F. Ehrburger-Dolle, *Electrical conductivity of carbon black-polyethylene composites - Experimental evidence of the change of cluster connectivity in the PTC effect.* Carbon, 2001. **39**(3): p. 375-382.
72. Belina, G., V. Urban, E. Straube, W. Pyckhout-Hintzen, M. Kluppel, and G. Heinrich, *Microscopic deformation of filler particles in rubber under uniaxial deformation.* Macromolecular Symposia, 2003. **200**: p. 121-128.
73. Bastide, J., L. Leibler, and J. Prost, *Scattering by Deformed Swollen Gels - Butterfly Isointensity Patterns.* Macromolecules, 1990. **23**(6): p. 1821-1825.
74. Morfin, I., F. Ehrburger-Dolle, I. Grillo, F. Livet, and F. Bley, *ASAXS, SAXS and SANS investigations of vulcanized elastomers filled with carbon black.* Journal of Synchrotron Radiation, 2006. **13**: p. 445-452.
75. Ehrburger-Dolle, F., F. Bley, E. Geissler, F. Livet, I. Morfin, and C. Rochas, *Filler networks in elastomers.* Macromolecular Symposia, 2003. **200**: p. 157-167.
76. Ehrburger-Dolle, F., M. Hindermann-Bischoff, F. Livet, F. Bley, C. Rochas, and E. Geissler, *Anisotropic ultra-small-angle X-ray scattering in carbon black filled polymers.* Langmuir, 2001. **17**(2): p. 329-334.
77. E. Geissler and F. Ehrburger-Dolle, private communication
78. Kohlbrecher, J., J. Buitenhuis, G. Meier, and M. Lettinga, *Colloidal dispersions of octadecyl grafted silica spheres in toluene: A global analysis of small angle neutron scattering contrast variation and concentration dependence measurements.* J Chem Phys, 2006. **125**: p. 044715.
79. Schaefer, D.W., J.E. Mark, D. Mccarthy, L. Jian, C.C. Sun, and B. Farago, *Structure of microphase -separated silica/siloxane molecular composites*. Material Research Society Symposium, ed. D.W. Schaefer and J.E. Mark. Vol. 171. 1991. 57-63.
80. Inoubli, R., S. Dagreou, A. Lapp, L. Billon, and J. Peyrelasse, *Nanostructure and mechanical properties of polybutylacrylate filled with grafted silica particles.* Langmuir, 2006. **22**(15): p. 6683-6689.
81. Oberdisse, J., *Aggregation of colloidal nanoparticles in polymer matrices.* Soft Matter, 2006. **2**(1): p. 29-36.
82. Oberdisse, J., *Structure and rheological properties of latex-silica nanocomposite films: Stress-strain isotherms.* Macromolecules, 2002. **35**(25): p. 9441-9450.
83. Oberdisse, J. and F. Boue, *Rheology-structure relationship of a model nanocomposite material.* Progress in Colloid and Polymer Science, 2004. **136**: p. 124-129.
84. Oberdisse, J. and B. Deme, *Structure of latex-silica nanocomposite films: A small-angle neutron scattering study.* Macromolecules, 2002. **35**(11): p. 4397-4405.

85. Oberdisse, J., A. El Harrak, G. Carrot, J. Jestin, and F. Boue, *Structure and rheological properties of soft-hard nanocomposites: influence of aggregation and interfacial modification.* Polymer, 2005. **46**(17): p. 6695-6705.
86. McCarthy, D.W., J.E. Mark, S.J. Clarson, and D.W. Schaefer, *Synthesis, structure, and properties of hybrid organic-inorganic composites based on polysiloxanes. II. Comparisons between poly(methylphenylsiloxane) and poly(dimethylsiloxane), and between titania and silica.* Journal of Polymer Science Part B-Polymer Physics, 1998. **36**(7): p. 1191-1200.
87. McCarthy, D.W., J.E. Mark, and D.W. Schaefer, *Synthesis, structure, and properties of hybrid organic-inorganic composites based on polysiloxanes. I. Poly(dimethylsiloxane) elastomers containing silica.* Journal of Polymer Science Part B-Polymer Physics, 1998. **36**(7): p. 1167-1189.
88. Schaefer, D.W., C. Suryawanshi, P. Pakdel, J. Ilavsky, and P.R. Jemian, *Challenges and opportunities in complex materials: silica-reinforced elastomers.* Physica a-Statistical Mechanics and Its Applications, 2002. **314**(1-4): p. 686-695.
89. Berriot, J., H. Montes, F. Martin, M. Mauger, W. Pyckhout-Hintzen, G. Meier, and H. Frielinghaus, *Reinforcement of model filled elastomers: synthesis and characterization of the dispersion state by SANS measurements.* Polymer, 2003. **44**(17): p. 4909-4919.
90. Berriot, J., F. Lequeux, L. Monnerie, H. Montes, D. Long, and P. Sotta, *Filler-elastomer interaction in model filled rubbers, a H-1 NMR study.* Journal of Non-Crystalline Solids, 2002. **307**: p. 719-724.
91. Berriot, J., F. Lequeux, H. Montes, and H. Pernot, *Reinforcement of model filled elastomers: experimental and theoretical approach of swelling properties.* Polymer, 2002. **43**(23): p. 6131-6138.
92. Berriot, J., H. Montes, F. Lequeux, D. Long, and P. Sotta, *Gradient of glass transition temperature in filled elastomers.* Europhysics Letters, 2003. **64**(1): p. 50-56.
93. Montes, H., F. Lequeux, and J. Berriot, *Influence of the glass transition temperature gradient on the nonlinear viscoelastic behavior in reinforced elastomers.* Macromolecules, 2003. **36**(21): p. 8107-8118.
94. Fleer, G., M. Cohen Stuart, J. Scheutjens, T. Cosgrove, and B. Vincent, *Polymers at interfaces*. 1st ed. 1993, New York: Chapman & Hall.
95. Rieger, J., E. Hadicke, G. Ley, and P. Lindner, *Crystals Made of Close-Packed Polymeric Spheres - a Neutron-Scattering Study on Latex Films.* Physical Review Letters, 1992. **68**(18): p. 2782-2785.
96. Chevalier, Y., C. Pichot, C. Graillat, M. Joanicot, K. Wong, J. Maquet, P. Lindner, and B. Cabane, *Film Formation with Latex-Particles.* Colloid and Polymer Science, 1992. **270**(8): p. 806-821.
97. Joanicot, M., K. Wong, and B. Cabane, *Interdiffusion in cellular latex films.* Macromolecules, 1996. **29**(14): p. 4976-4984.
98. Winnik, M.A., *Latex film formation.* Current Opinion in Colloid & Interface Science, 1997. **2**(2): p. 192-199.
99. Rharbi, Y., F. Boue, M. Joanicot, and B. Cabane, *Deformation of cellular polymeric films.* Macromolecules, 1996. **29**(12): p. 4346-4359.
100. Rharbi, Y., B. Cabane, A. Vacher, M. Joanicot, and F. Boue, *Modes of deformation in a soft hard nanocomposite: A SANS study.* Europhysics Letters, 1999. **46**(4): p. 472-478.
101. Grillet, A.C., S. Brunel, Y. Chevalier, S. Usoni, V. Ansanay-Alex, and J. Allemand, *Control of the morphology of waterborne nanocomposite films.* Polymer International, 2004. **53**(5): p. 569-575.

102. Shinohara, Y., H. Kishimoto, K. Inoue, Y. Suzuki, A. Takeuchi, K. Uesugi, N. Yagi, K. Muraoka, T. Mizoguchi, and Y. Amemiya, *Characterization of 2D-USAXS Apparatus for Application of Rubber Filled with Spherical Silica under Elongation.* J. Appl. Cryst., 2007. **40**: p. s397-s401.
103. Ikeda, Y., Y. Yasuda, S. Yamamoto, and Y. Morita, *Study on 2D-SAXS of in situ silica filled nanocomposite elastomer during deformation.* J. Appl. Cryst., 2007. **40**: p. s549-s552.
104. Le Diagon, Y., S. Mallarino, and C. Fretigny, *Particle structuring under the effect of an uniaxial deformation in soft/hard nanocomposites.* European Physical Journal E, 2007. **22**: p. 77-83.
105. McGreevy, R.L. and P. Zetterstrom, *To RMC or not to RMC? The use of reverse Monte Carlo modelling.* Current Opinion in Solid State & Materials Science, 2003. **7**(1): p. 41-47.
106. Pusztai, L., H. Dominguez, and O.A. Pizio, *Reverse Monte Carlo modeling of the structure of colloidal aggregates.* Journal of Colloid and Interface Science, 2004. **277**(2): p. 327-334.
107. Radhakrishnan, B., R. Ranjan, and W.J. Brittain, *Surface initiated polymerizations from silica nanoparticles.* Soft Matter, 2006. **2**(5): p. 386-396.
108. El Harrak, A., G. Carrot, J. Oberdisse, J. Jestin, and F. Boue, *Control of the colloidal stability of polymer-grafted-silica nanoparticles obtained by atom transfer radical polymerization.* Macromolecular Symposia, 2005. **226**: p. 263-278.
109. El Harrak, A., G. Carrot, J. Oberdisse, J. Jestin, and F. Boue, *Atom transfer radical polymerization from silica nanoparticles using the 'grafting from' method and structural study via small-angle neutron scattering.* Polymer, 2005. **46**(4): p. 1095-1104.
110. Kawasumi, M., *The discovery of polymer-clay hybrids.* Journal of Polymer Science Part a-Polymer Chemistry, 2004. **42**(4): p. 819-824.
111. Hermes, H.E., H. Frielinghaus, W. Pyckhout-Hintzen, and D. Richter, *Quantitative analysis of small angle neutron scattering data from montmorillonite dispersions.* Polymer, 2006. **47**(6): p. 2147-2155.
112. Loizou, E., P. Butler, L. Porcar, E. Kesselman, Y. Talmon, A. Dundigalla, and G. Schmidt, *Large scale structures in nanocomposite hydrogels.* Macromolecules, 2005. **38**(6): p. 2047-2049.
113. Causin, V., C. Marega, A. Marigo, and G. Ferrara, *Assessing organo-clay dispersion in polymer layered silicate nanocomposites: A SAXS approach.* Polymer, 2005. **46**(23): p. 9533-9537.
114. Vaia, R.A. and W.D. Liu, *X-ray powder diffraction of polymer/layered silicate nanocomposites: Model and practice.* Journal of Polymer Science Part B-Polymer Physics, 2002. **40**(15): p. 1590-1600.
115. Hanley, H.J.M., C.D. Muzny, D.L. Ho, and C.J. Glinka, *A small-angle neutron scattering study of a commercial organoclay dispersion.* Langmuir, 2003. **19**(14): p. 5575-5580.
116. Kratky, O. and G. Porod, J Coll Sci, 1949. **4**: p. 35.
117. Causin, V., C. Marega, A. Marigo, G. Ferrara, G. Idiyatullina, and F. Fantinel, *Morphology, structure and properties of a poly(1-butene)/montmorillonite nanocomposite.* Polymer, 2006. **47**(13): p. 4773-4780.
118. Benetti, E.M., V. Causin, C. Marega, A. Marigo, G. Ferrara, A. Ferraro, M. Consalvi, and F. Fantinel, *Morphological and structural characterization of polypropylene based nanocomposites.* Polymer, 2005. **46**(19): p. 8275-8285.

119. Chevalier, Y., M. Hidalgo, J.Y. Cavaille, and B. Cabane, *Structure of waterborne organic composite coatings.* Macromolecules, 1999. **32**(23): p. 7887-7896.
120. Colombini, D., H. Hassander, O.J. Karlsson, and F.H.J. Maurer, *Influence of the particle size and particle size ratio on the morphology and viscoelastic properties of bimodal hard/soft latex blends.* Macromolecules, 2004. **37**(18): p. 6865-6873.
121. Fahrlander, M., M. Bruch, T. Menke, and C. Friedrich, *Rheological behavior of PS-melts containing surface modified PMMA-particles.* Rheologica Acta, 2001. **40**(1): p. 1-9.
122. Bates, F.S., R.E. Cohen, and C.V. Berney, *Small-Angle Neutron-Scattering Determination of Macro-Lattice Structure in a Polystyrene Polybutadiene Diblock Co-Polymer.* Macromolecules, 1982. **15**(2): p. 589-592.
123. Inoue, T., M. Moritani, Hashimot.T, and H. Kawai, *Deformation Mechanism of Elastomeric Block Copolymers Having Spherical Domains of Hard Segments under Uniaxial Tensile Stress.* Macromolecules, 1971. **4**(4): p. 500-&.
124. Seguela, R. and J. Prud'homme, *Deformation mechanism of thermoplastic two-phase elastomers of lamellar morphology having a high volume fraction of rubbery microphase.* Macromolecules, 1981. **14**(1): p. 197-202.
125. Seguela, R. and J. Prud'homme, *Affinity of grain deformation in mesomorphic block polymers submitted to simple elongation.* Macromolecules, 1988. **21**(3): p. 635-643.
126. Corte, L., V. Rebizant, G. Hochstetter, F. Tournilhac, and L. Leibler, *Toughening with Little Stiffness Loss: Polyamide Filled with ABC Triblock Copolymers.* Macromolecules, 2006. **39**(26): p. 9365-9374.
127. Blundell, D.J., G. Eeckhaut, W. Fuller, A. Mahendrasingam, and C. Martin, *Real time SAXS/stress-strain studies of thermoplastic polyurethanes at large strains.* Polymer, 2002. **43**(19): p. 5197-5207.